MATHEMATICAL MODELING OF WORMHOLE PROPAGATION DURING MATRIX ACIDIZING OF CARBONATE RESERVOIRS

A Dissertation

by

OLATOKUNBO OLABODE AKANNI

Submitted to the Office of Graduate and Professional Studies of
Texas A&M University
in partial fulfillment of the requirements for the degree of

DOCTOR OF PHILOSOPHY

Chair of Committee,	Hisham A. Nasr-El-Din
Committee Members,	Maria A. Barrufet
	Jerome Schubert
	Mahmoud El-Halwagi
Head of Department,	A. Daniel Hill

December 2015

Major Subject: Petroleum Engineering

ABSTRACT

This study demonstrates the application of an alternative formulation to effectively describe the flow field in a two-scale carbonate matrix-acidizing model. The model is further modified and extended to alternative acidizing fluids such as chelates and organic acids. Existing carbonate acidizing models in the literature are analyzed for their accuracy in field-scale application, and recommendations are made for the best methods for obtaining optimum injection and wormhole propagation rates. Finally, a selection procedure for acids and additives is developed to aid in designing an optimal carbonate matrix acid treatment.

The fluid field flow in this two-scale model is described by the Navier-Stokes momentum formulation. The model is implemented via a commercial computational fluid dynamics package to solve the momentum, mass conservation, and species transport equations in the Darcy scale. The software is combined with functions and routines written in the C programming language to solve the porosity evolution equation, update the pore scale parameters at every time step in the simulation, and couple the Darcy and pore scales. A nonlinear kinetics equation which accounts for the weak dissociation of organic acid is used to describe the reaction of acetic acid with limestone in the modified model.

The output from the model is consistent with experimental observations, and the results from various sensitivity tests performed are in agreement with previously developed two-scale models based on the Darcy formulation. Numerical simulation results also showed that the optimum injection rate obtained in laboratory coreflood experiments

cannot be directly translated for field applications due to the effect of flow geometry and medium dimensions on the wormholing process. The simulation runs from the modified model for acetic acid produced output that matched experimental results, but the output for chelating agents does not quantitatively match with experimental results.

The model in this work is computationally less expensive than previous Darcy-Brinkman-based model. The simulations at very high injection rates with this model require less computational time than those developed with the Darcy formulation. For field treatment, it is recommended to inject the acid at the maximum allowable rate, and monitor wormhole propagation using the modified semi-empirical model.

DEDICATION

I dedicate this work to the omniscient God and also to my lovely family:

Olufolake and Ifeoluwapo.

ACKNOWLEDGEMENTS

I would like to express my heartfelt gratitude to my committee chair and advisor, Dr. H.A. Nasr-El-Din, for his indispensable guidance and unwavering support throughout the course of this study. He has been an excellent mentor to me. His passion and drive for continued discovery of knowledge and excellence has been an inspiration for me to be the best I can be at my work every day.

I also thank my committee members, Dr. M.A. Barrufet, Dr. J. Schubert, and Dr. M. El-Halwagi, for accepting to serve on my committee and for their support.

I want to extend my appreciation to CARBO Ceramics for providing financial support for parts of this study and to the Texas A&M University High Performance Research Computing Facility for granting access to their computer resources during the course of my research. I also appreciate Gia Alexander for proofreading my dissertation.

This study would not have been possible without my family. Thanks to my dad Olusola and my mother Bosede for their support and encouragement, my brother Oluyemi for paving the way, and finally to my lovely wife Olufolake and precious daughter Ifeoluwapo.

NOMENCLATURE

A_1	constant used in calculating dissociation constant, T, °K
A_2	constant used in calculating dissociation constant, dimensionless
A_1	constant used in calculating dissociation constant, 1/T, 1/°K
AR	aspect ratio, dimensionless
a_o	initial interfacial area per unit volume of the medium, 1/L, m^{-1}
a_v	interfacial area per unit volume of the medium, 1/L, m^{-1}
a_{H+}	activity coefficient of hydrogen ion, dimensionless
a_{A-}	activity coefficient of conjugate base of acid, dimensionless
c_1, c_2	experimentally determined model coefficients, dimensionless
d_1, d_2	experimentally determined model coefficients, dimensionless
C_f	original concentration of acid in the fluid phase, n/L^3, mol/L
C_s	concentration of acid at the solid-fluid interface, n/L^3, mol/L
d	diameter of core, L, m [in.]
D	fluid diffusivity in mixed rock formation, L^2/t, cm^2/s [m^2/s]
$d_{e,wh}$	effective diameter of wormhole cluster, L, ft [m]
D_e	effective dispersion tensor, L^2/t, m^2/s
D_{eX}	effective longitudinal dispersion coefficient, L^2/t, m^2/s
D_{eT}	effective transverse dispersion coefficient, L^2/t, m^2/s
dl%	percentage of dolomite in rock, percentage
D_m	acid diffusivity, L^2/t, m^2/s

ΔE	activation energy, $mL^2/t^2/mol$, kJ/mol
E_f	reaction rate constant, $n^{(1-n)}/L^{(n-1)}t^{-1}$, $mol^{(1-n)}/m^{(n-1)}s^{-1}$
h	total thickness of reservoir, L, ft [m]
I_{ani}	measure of horizontal to vertical permeability anisotropy, dimensionless
K	permeability tensor, L^2, m^2 [md]
k_c	local mass transfer coefficient, L/t, m/s [cm/s]
$k_{cP,}$	mass transfer coefficients for products, L/t, m/s [cm/s]
k_{cR}	mass transfer coefficients for reactants, L/t, m/s [cm/s]
k_d	dissociation constant, dimensionless
k_{eff}	effective reaction rate constant, L/t, m/s [cm/s]
K_{eq}	reaction-equilibrium, dimensionless
k_H	horizontal permeability, L^2, m^2 [md]
K_o	initial permeability tensor, L^2, m^2 [md]
k_s	surface dissolution reaction-rate constant, L/t, m/s
k_V	vertical permeability, L^2, m^2 [md]
L	length of wormhole, L, m [cm]
L_{core}	core length, L, m [in.]
L_h	horizontal well, length, L, ft [in.]
ls%	percentage of limestone in rock, percentage
m_{wh}	number of dominant wormholes along the angular direction, dimensionless
n	order of reaction, dimensionless
N_{ac}	acid capacity number, dimensionless

N_{Da}	Damköhler number, dimensionless
N_{pe}	Péclet number, dimensionless
p	pressure, m/L^2t^2, psi [MPa]
$\bar{p}$	average reservoir pressure, m/L^2t^2, psi [MPa]
p_f	fracture pressure, m/L^2t^2, psi [MPa]
$PV_{bt,\ opt}$	optimum pore volume to breakthrough, dimensionless
PV_{BT}	pore volumes of acid injection to breakthrough, dimensionless
Q	acid injection rate, L^3/t, bbl/d
Q_{max}	maximum allowable injection rate, L^3/t, bbl/d
q_{opt}	optimum acid injection rate, L^3/t, bbl/d
R	gas constant, $L^2m/molt^2T$, J/Kmol
R(C)	reaction kinetics, n/tL^2, $mol/s/m^2$
r_e	drainage radius, L, m, ft [in.]
Re_p	Reynolds number, dimensionless
r_o	initial pore radius, L, m
r_p	pore radius, L, m
r_w	wellbore radius, L, m, ft [in.]
S	total skin value, dimensionless
Sc	Schmidt number, dimensionless
Sh	Sherwood number, dimensionless
Sh_∞	asymptotic Sherwood number, dimensionless
T	temperature, T, °C [°K]

t	time, t, s
u	superficial velocity vector, L/t, m/s [cm/s]
u_o	inlet Darcy velocity, L/t, m/s [cm/s]
u_{opt}	optimum injection velocity, L/t, m/s [cm/s]
ν	stoichiometric ratio of products to reactants, dimensionless
$v_{i,opt}$	optimum interstitial velocity, , L/t, m/s [cm/s]
v_{wh}	wormhole propagation rate, L/t, m/s [cm/s]
z_w	elevation of well from reservoir bottom, L, ft [m]
α	dissolving power of acid, m/n, g/mol
α_{os}	constant in dispersion correlations, dimensionless
α_z	wormhole axial spacing coefficient, dimensionless
β	pore structure relation constant, dimensionless
γ	parameter for fluid-loss-limited wormholing, dimensionless
$\Delta\varepsilon$	porosity heterogeneity magnitude, dimensionless
$\Delta\varepsilon_c$	critical porosity heterogeneity magnitude, dimensionless
ε	porosity of the medium, dimensionless
ε_o	initial porosity, dimensionless
κ	overall dissolution rate constant, L/t, m/s [cm/s]
ρ	fluid density, m/L^3, kg/m^3 [g/cm^3]
ρ_s	rock density, m/L^3, kg/m^3 [g/cm^3]
λ_X	constant in axial dispersion correlation, dimensionless
λ_T	constant in transverse dispersion correlation, dimensionless

μ	fluid viscosity, m/Lt ,mPa.s [cp]
μ_o	specific fluid viscosity, m/Lt ,mPa.s [cp]
ν	kinematic viscosity, L^2/t, m^2/s [cSt]
τ	stress tensor, m/L^2t^2, psi [MPa]

TABLE OF CONTENTS

Page

LIST OF FIGURES

Page

LIST OF TABLES

Page

1 INTRODUCTION

1.1. Overview

Matrix acidizing of wells with acid is a widely used practice to enhance the inflow of hydrocarbon to the wellbore. The process involves injecting an acidizing fluid into the formation, below the formation fracture pressure, to improve the permeability near the wellbore. In carbonate reservoirs, the acidizing fluid is injected to create conductive flow channels that extend beyond the formation damage or region of low permeability near the wellbore, thereby increasing the inflow performance of the well. These conductive flow channels created by the acid in carbonate formations are called wormholes. **Fig. 1.1** illustrates acidizing fluid enlarges the pores during the acid treatment of carbonate formation to create wormholes that penetrate deep into the rock as desired.

The post-treatment skin factor of carbonate reservoirs could be negative (if the flow channels penetrate past the damage zone in the formation) signifying an improvement over the original skin factor.

Wormholes form in a dissolution process during an efficient carbonate matrix treatment. As the acid is injected at a certain optimum rate, the large pores grow at a higher rate than the smaller pores, the larger pores receive an increasing portion of the acidizing fluid during the process, which increases their length and volume and eventually become wormholes. Wormholes do not necessarily form in the dissolution of carbonate rock with an acid; the dissolution structure is mainly a function of the injection rate and also the fluid-mineral properties, which includes the reaction kinetics, mass transfer rates, the flow

geometry, and the fluid loss rate. The possible dissolution structures formed during carbonate matrix acidizing are face dissolution, conical wormholes, dominant wormholes, ramified wormholes, and uniform dissolution.

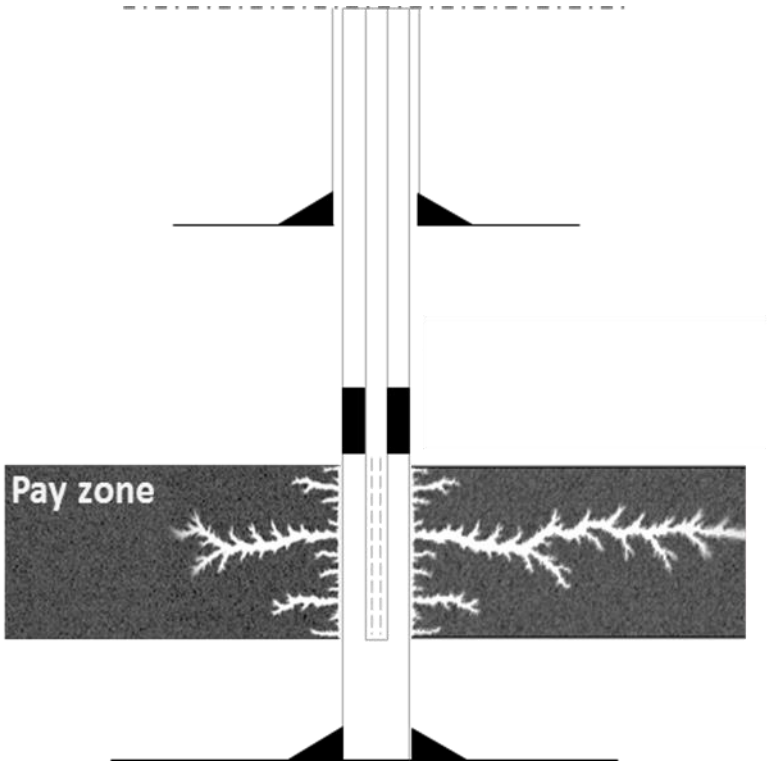

Fig. 1.1–Wormholes are formed during an efficient acid treatment by the acid enlarging the pores and creating connecting flow channels in the formation.

When the acidizing fluid is injected at very low rates in laboratory coreflood tests, the fluid is consumed at the inlet face of the core before it can penetrate the rock, resulting in face dissolution and a high volume of the fluid is required to achieve breakthrough at the outlet. At slightly higher injection rates, a conical-shaped dissolution channel is formed

as significant amounts of the acidizing fluid are consumed on the walls of the wormholes and the fluid penetrates into the rock and enlarges flow channels. At intermediate flow rates (optimum injection rate) the fluid is transported to the tip of the developing flow channel and propagates the medium, leading to the establishment of a dominant wormhole.

When the injection rate is higher than the optimum rate, the fluid is forced into smaller pores and the enlarged pores become more branched resulting in ramified wormhole patterns. At very high rates, the fluid penetrates into the medium but is not completely spent due to insufficient resident time, which leads to uniform dissolution patterns and unsuccessful treatment in field conditions. An acid efficiency curve is presented in **Fig. 1.2** showing the effect of injection rate on the possible dissolution patterns that can be formed during carbonate acidizing.

1.2. Purpose of Study

A successful matrix acidizing treatment reduces the skin of the well to at least its value before damage in the near-wellbore. Past studies show that more than 35% of matrix acidizing treatments resulted in failure or fell below expectations (Sengul and Remisio 2002) due to inadequately designed treatment procedure. A main factor in designing an effective carbonate acidizing matrix treatment is the assessment of dissolution patterns that will be formed by the fluid-mineral system.

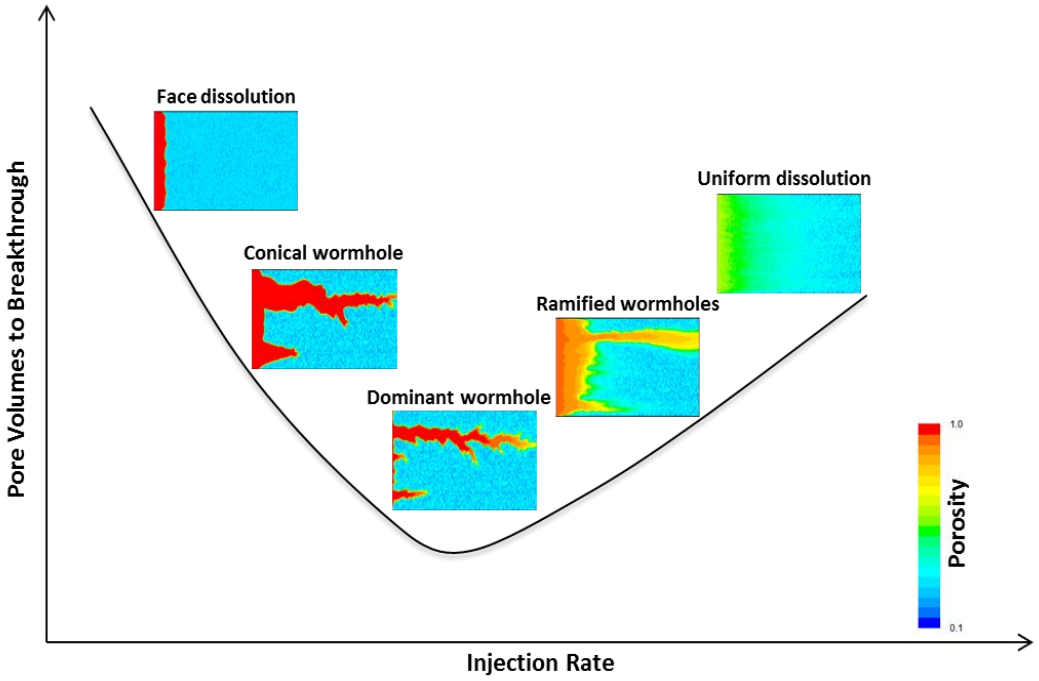

Fig. 1.2–Acid efficiency curve showing the effect of acid injection rate on dissolution patterns and the pore volumes of acid required to breakthrough.

The dissolution pattern affects the skin evolution because the pattern determines the depth of penetration of the acid into the rock. When dominant wormhole patterns are formed, the acid penetrates deepest into the formation which leads to the highest reduction in skin after treatment. Therefore, to obtain the best results from an acid stimulation treatment, it is important to inject the acid at the optimum injection rate for the particular fluid-mineral system (Akanni and Nasr-El-Din 2015). Carbonate acidizing models have been developed from past studies to properly understand the formation of wormholes and predict the optimum conditions for treatment design.

Most of the available carbonate acidizing models are designed only for the fluid-mineral combination of hydrochloric acid (HCl) and limestone due to the complex

chemistry of alternative acidizing fluids such as chelates and organic acids. Other limitations with existing models include incorrect scaling of linear core scale results to radial field scale applications, non-inclusion of additives in reaction rate calculations, and formation heterogeneity.

This first part of this study analyzes the existing carbonate matrix-acidizing models in the literature for their accuracy in predicting optimum injection rates, wormhole propagation rates, and dissolution patterns. The principles behind the development of these model equations and the major assumptions made in the models is also examined. The practicality in field scale applications and their technical limitations are also discussed.

The second part of this work develops a numerical model by modifying the two-scale approach (with fluid flow described by Navier-Stokes momentum formulation) to study the propagation of wormholes during carbonate acidizing. The model is then extended for other acidizing fluid systems. In addition, a comprehensive acid and additives selection system is developed for the design of an efficient carbonate matrix acidizing treatment based on the available well and reservoir information.

1.3. Dissertation Outline

This section gives an introduction to the problem and also provides the motivation of work and objective of study. Section 2 details an extensive literature review of carbonate acidizing models. It also includes recommendation of which model is best suited to calculate the optimum injection rate and wormhole propagation rate in field conditions.

Section 3 focuses on the description, development, and implementation of the two-scale model to study wormhole propagation during carbonate matrix acidizing.

Section 4 presents the analysis of results obtained from the modified model and comparison results with output from experimental findings and existing carbonate acidizing models. In Section 5, the two-scale model is extended for organic acids and chelating agents and the results are compared with reported trends from experiments. Section 6 shows the system designed for the selection of the acidizing fluid and additives for carbonate acidizing treatment, and Section 7 summarizes the contributions of this study with recommendations for future work.

2 CARBONATE MATRIX-ACIDIZING MODELS AND APPLICATIONS*

2.1. Literature Review

Numerous theoretical and experimental studies have been conducted in the past to understand the propagation of wormholes during carbonate matrix acidizing. From these studies, mathematical models were developed to predict the dissolution structure of the acid-rock reaction, the optimum injection rate for the most efficient treatment, and/or the propagation rate of the wormhole in the rock with volume injected to monitor the skin evolution during treatment. Fredd and Miller (2000) classified models for acid stimulation of carbonates into five categories based on the approach to solution. These categories, with two new ones, are used in this study to describe existing models. Glasbergen et al. (2009) reviewed some models which predicted optimum injection rates and examined the limitations of these models in translating their results from laboratory core-scale to field conditions. Brief reviews of some of these models can also be found in Schechter (1992), Golfier et al. (2002), and Panga et al. (2005).

The carbonate matrix-acidizing models existing in literature today can be broadly classified into the following seven categories: The capillary tube approach, Damköhler number approach, transition pore theory, network models, Péclet number approach, semi-empirical approach, and averaged continuum (or two-scale) models. Some models are

*Part of this section is reprinted with permission from "The Accuracy of Carbonate Matrix-Acidizing Models in Predicting Optimum Injection and Wormhole Propagation Rates" by Akanni, O. O. and Nasr-El-Din, H. A. 2015. SPE © Paper SPE 172575 presented at the SPE Middle East Oil & Gas Show and Conference. Manama, Bahrain. Further reproduction prohibited without permission.

based on more than one of the approaches listed, with the Damköhler number theory being the most often combined one. This will be discussed later as the different groups are reviewed.

2.1.1. Capillary Tube Approach

The wormhole is modeled as a cylindrical tube in this approach, with the wormhole assumed to already exist and the shape predetermined. The early models based on this approach simulated mass-transfer limited dissolution based on bundles of capillary tubes (Rowan 1959), with a focus on the effect of fluid leakage and the mechanism of transport and reaction in the wormhole. Schechter and Gidley (1969) extended this theory to include the effects of pore merging surface reaction limited dissolution. Hung et al. (1989), Wang et al. (1993), Buijse (1997), and Huang et al. (1997) have also developed models based on this approach. A fundamental limitation of these models is the assumption of the initial formation of the wormhole, thus, microscopic pore distribution (number of pores and radii on rock surface where acid is injected) is required to set up the model.

The Hung et al. (1989) model is only applicable to mass-transfer limited systems. The authors model the wormhole propagation rate as a function of injection rate, diffusion coefficient, and acid leakoff rate along the walls of the wormhole. The wormhole is modeled as a cylindrical pipe with porous walls, and as acid flows into the wormhole, it dissolves the rock surface and penetrates the rock matrix. Fluid leak off along the walls of the wormhole as acid propagates into the rock is also modeled. Mass balance equations are written for the wormhole propagation rate for the propagation rate of acid in both the axial and radial directions of propagation. They modeled multiple wormhole cases, and

for this, the initial condition for the model is the pore size distribution for the porous media. Wormholes are concluded to form from the largest pore or surface defects on the rock surface.

Buijse (1997) also modeled the wormhole as a cylindrical pore and numerically solved the resulting convection-diffusion equations. This model is applicable to both reaction-controlled and diffusion-controlled regimes by assuming a finite acid-rock reaction rate to enable the calculation of spending profiles in both of these regimes. Fluid loss from wormholes to the formation is ignored in the modeling of acid flow and the reaction as a cylindrical pore. The model does not predict wormhole geometry or skin evolution during treatment and would require wormhole density to be translated to field scale.

Using the capillary tube approach, Gdanski (1999) described the formation of wormholes and explored the following three areas regarding wormhole formation: The number of dominant wormholes created, the spatial distribution of those dominant wormholes along the wellbore, and the fluid leakoff profile from the dominant wormholes under radial conditions. Several simplifying assumptions are made in this model based on the experimentally observed symmetrical nature of the wormhole formation under radial flow conditions.

Huang et al. (1999) used the capillary tube approach to predict wormhole population density and calculate the volume of acid required to create wormholes of a certain density and length. According to the authors, the disturbance of local pressure distribution when wormhole is initiated at any point along the wellbore results in lower

pressure gradients in the wormholes surrounding region. They numerically simulated the flow field around a wellbore with a wormhole extending into the formation to quantify the development of wormholes and the associated pressure distribution. From this, they then developed a model to predict the wormhole density along a wellbore as a function of the acidizing conditions.

2.1.2. Damköhler Number Approach

The Damköhler number is defined as the ratio of the net rate of acid dissolution to the rate of transport of acid by convection. The net rate of dissolution is the rate of mass transfer for mass-transfer limited systems or the rate of surface reaction for reaction-rate limited systems. Initial studies by Hoefner and Fogler (1988) showed that the wormhole formation process is controlled by the Damköhler number. The effect of the Damköhler number on the wormhole structure was investigated and confirmed by their experimental work, and they also demonstrated the effect of the wormhole structure on the successful outcome of matrix acid treatments.

Fredd and Fogler (1998, 1999) conducted further studies on the effects of transport and reaction on the formation of wormholes for weak acids, strong acids, and chelating agents. They showed that these fluid systems are influenced by various transport and reaction mechanisms, and when both mechanisms are taken into account, a common dependence on the Damköhler number was observed. There exists an optimum Damköhler number at approximately 0.29 for all the fluid-mineral systems they investigated. This is the Damköhler number at which a minimum number of pore volumes are required for channel breakthrough in the coreflood test conducted. Their work also included the effect

of temperature on wormhole formation, showing that the optimum injection rate increased with increasing temperature.

Fredd and Fogler (1999) observed that the wormhole pattern and the amount of acid injected to breakthrough in a coreflood test are influenced by a dimensionless kinetic parameter, which they defined as the ratio of the surface reaction to the overall rate of dissolution. An optimum kinetic parameter of 130, at which wormhole formation becomes most efficient, is reported. The models based on the Damköhler number theory need to be combined with other models to predict skin evolution because they do not independently predict wormhole growth. Wormhole density and dimensions are required because the Damköhler number only applies to a single wormhole for a linear coreflood test, and it does not translate directly to field scale.

To address this issue of scaling laboratory data to field and skin monitoring, Fredd (2000) developed a dynamic model which extended the works of Fredd and Fogler (1998, 1999) by including the effects of wormhole competition and fluid loss through the wormhole walls. The model was based on a capillary tube representation of the dominant wormholes. Fluid loss from the wormhole walls was included, and the effects of transport and reaction on channel evolution were determined based on the Damköhler number and kinetic parameters. The model is based on three main assumptions: (1) Fluid loss or wormhole competition do not influence the dependence of wormhole formation on the Damköhler number and the kinetic parameter, (2) the rate of fluid loss is consistent with that predicted for a single wormhole, and (3) the number of wormholes per unit volume

of rock is consistent with laboratory data and follows the scaling rule from network model simulations.

2.1.3. Transition Pore Theory

This theory was originally developed by Wang et al. (1993) to calculate the optimum flux to generate dominant wormholes during a matrix acid treatment. According to their studies, large pores must be present in virgin rock for wormholing to be initiated for a mass controlled process. If all pores in the formation are so small that the process is reaction controlled, then they will initially dissolve uniformly and wormholes will not form until some of the pores have reached a critical size. They postulated that there exists a critical pore cross-sectional area on the face of the rock for the formation of wormholes. An expression was obtained from the growth rate functions, based on previous work by Schechter and Gidley (1969), which relates the optimum acid flux with the Damköhler number and emphasizes the effects of rock mineralogy, reaction temperature, and acid concentration. This method requires microscopic pore description for implementation; it cannot be applied for monitoring skin evolution during treatment, and it erronously predicts that an increase in acid concentration will decrease the optimal acid flux (Fredd and Miller 2000).

Huang et al. (1997) included a fluid loss model with the transition pore theory to translate the results from laboratory core scale to field scale. According to their study, the optimal acid flux observed in a wide range of experiments compared favorably with the values predicted by the transition pore theory model. However the fluid loss from wormholes in a field treatment is higher than that of coreflood tests and the direct

extrapolation of wormhole propagation rates from coreflood tests to field design will over predict wormhole propagation for field treatments. The equation presented gives reasonable optimum acid flux values at room temperatures, but the values become exaggerated as the temperature increases. The model exhibits the same basic limitations also observed in the Wang et al. (1993) publication.

2.1.4. Network Model Approach

The network approach has been used by various investigators to describe processes in porous media where the relevant structural property of pore interconnectedness must be included. It was first introduced by Fatt (1956) and, according to Hoefner and Fogler (1988), has been employed successfully to include fluid displacement (Simon and Kesley 1972), relative permeability (Rose 1957), and dispersion in porous media (Sahimi et al. 1990).

Hoefner and Fogler (1988) carried out a theoretical study on the dissolution of porous media by flowing acid using this approach, also combining their work with experimental observations. The network approach considers the dissolution of the grains of the solid in a two-dimensional structure, and the space between two pores is represented by a cylindrical capillary. To model wormhole behavior, the acid concentration in each capillary is calculated and the radii of the capillaries are increased as dissolution occurs. The average flow rate is assumed to be proportional to the pressure difference and the dissolution is assumed to be proportional to the average velocity and concentration. Dissolution is assumed to occur by first-order heterogeneous chemical reactions. The model also assumes there is no merging of pores during the propagation of wormholes,

and this may lead to misrepresentation of the model in the fluid zone. This model does not readily scale to field or laboratory experiments due to the limited number of pores.

Fredd and Fogler (1998) extended the works of Bryant et al. (1993) and Thompson and Fogler (1997) of a 3D physically representative network (PRN) model to simulate the effects of transport and reaction on the formation of wormholes. The PRN model is based on a 3D packed bed representation of the porous medium. The bed is generated from the physical properties of the bed using a drop-and-roll algorithm, which simulates the random packing in a specified volume. The 2D network model modeled transport and reaction of the fluid in porous medium similar to the PRN model. They reported their simulations qualitatively matched with experimental results and also demonstrated the existence of an optimum Damköhler number. The PRN model requires large computational power to be applicable at field or laboratory scale, and this is not available for practical application.

2.1.5. Péclet Number Approach

Daccord et al. (1989) presented a model which quantifies wormholes by a unique parameter, their equivalent hydraulic length. This method is based on correlations at the scale of the core sample and the physical parameters involved in the problem are introduced in the form of dimensionless numbers. The model postulates that the propagation of wormholes is a function of the Péclet number (Npe), the injection volume, and a fractal dimension. In developing the growth rate equation for the radial case, it is assumed that the effect of a finite wellbore radius is equivalent to pumping an extra volume of fluid equal to that necessary to get a penetration equal to the wellbore radius.

Frick et al. (1994) extended the work of Daccord et al. (1989) by also considering wormholes as fractals. The influences of acid volume, injection rate, fractal dimension, porosity, and the ratio of undamaged to damaged permeability on well performance are factored in. They developed equations for the calculation of post-treatment skin effects for vertical and horizontal wells. They concluded that the exponent of the Péclet number is critical and influences the orders of magnitude of the required acid volume for reduction of a given skin effect. The results of their study suggest that the injection rate has no major effect on the dissolution patterns.

2.1.6. Semi-Empirical Approach

Buijse and Glasbergen (2005) took a different approach by describing a relatively simple model to capture the essential physics and chemistry of the wormholing process. The growth rate of the wormhole front was modeled as a function of the interstitial velocity of the acid, which is a function of acid injection rate. In this semi-empirical model, parameters such as permeability, mineralogy, temperature, and acid concentration are not modeled explicitly but incorporated in the model in the form of two constants calculated from the optimum acid velocity and pore volume to breakthrough at this velocity. These constants are obtained from coreflood tests for the fluid-mineral system being investigated.

In developing a radial analogue of the linear wormhole model, it is assumed that the functional relationship between the interstitial velocity and the velocity of the wormhole front as observed in coreflood tests holds for radial geometry. It is also assumed that the permeability of the treated zone after stimulation is at least an order of magnitude

larger than the original permeability (in calculating the post-treatment skin). To model fluid distribution and wormhole growth in a heterogeneous formation, this model must be embedded into a more comprehensive near-wellbore simulator.

Furui et al. (2012) extended the semi-empirical correlation model by Buijse and Glasbergen (2005) and combined it with the earlier described capillary tube model (Hung et al. 1989), which is based on acid transport and fluid loss from a single wormhole. This model improves on the previous semi-empirical one by accounting for the effect of core size used in the coreflood test, from which the parameters used in the model are obtained. Wormhole growth is related to the in-situ injection velocity at the tip of the dominant wormhole, and at sufficiently high injection velocity, the acid concentration at the wormhole tip is assumed to be equal to the acid concentration (at injection point). The effective surface area available for the acid reaction is assumed to be proportional to the wormhole penetration length. The results of this model depend on the efficiency of the coreflood experiments, from which the main parameters used in the equations are obtained. Any shortcoming in the laboratory result will bias the output of the model.

2.1.7. Averaged Continuum (Two-Scale) Models

In the two-scale (averaged-continuum) approach, the transport and reaction of the acidizing fluid is modeled as an interaction between the Darcy scale and the pore scale. Liu et al. (1997) developed an approach based on continuum equations written at Darcy's scale. The model is based on solving the equations of fully coupled fluid flow, reactants transport, and rock-fluid reactions which includes the effect of rock dissolution with porosity and permeability changes in the pore scale due to the mineral-acid reaction. This

method was developed primarily for sandstones, but the model also captures the wormholing pattern for carbonate formations. This model is based on the assumption that the dissolution is reaction-rate controlled and is valid only in the kinetic regime; the effect of mass transfer on the reaction rate is not considered.

Golfier et al. (2002) extended the work done by Liu et al. (1997) to develop a Darcy-scale model to describe the dissolution of carbonates. At every time step in the simulation of the model, a mass transfer coefficient is calculated from a pore scale simulation to couple the pore scale to the Darcy scale. A completely mass transfer controlled reaction is assumed in the model, which effectively captures qualitative and quantitative features of the dissolution patterns in this regime.

Panga et al. (2004, 2005) also worked further on the two-scale continuum model for describing wormhole initiation and propagation in carbonates. The following three dimensionless parameters are defined in their model: Thiele modulus (pore scale parameter), Damköhler number (core scale parameter), and the acid capacity number (dependent on the fluid-mineral system). The model was also used to investigate the effect of dispersion, rock heterogeneities, reaction kinetics, and mass transfer on the formation of wormholes. This model is applicable to simulate linear flow but does not accurately describe radial flow to translate to field conditions.

Kalia and Balakotaiah (2007) built on the work by Panga et al. (2005) to simulate the radial flow in the model. The authors investigated the effects of convection and diffusion on dissolution patterns, and also that of rock heterogeneities on wormhole propagation in the radial model. Kalia and Balakotaiah (2009) studied the effect of

heterogeneities of the porous medium on the dissolution patterns formed during a carbonate acidizing process using the two-scale model.

Further work by Maheshwari et al. (2012) was done to extend the two-scale model by Kalia and Balakotaiah (2007, 2008) for 3D simulation. Sensitivity analysis of the dissolution process to the acid injection rate, reaction rate constant, initial average permeability, heterogeneity, and permeability-porosity relationships were carried out. This model was extended to be made applicable for gelled acids by Ratnakar et al. (2012), in which the two-scale model is combined with a semi-empirical rheological model that accounts for viscosity as a function of pH, shear rate and temperature. This was also employed for emulsified acids by Maheshwari et al. (2014).

Other applications of the two-scale approach have been made by various investigators. De Oliveira et al. (2012) used the model to investigate the effect of mineralogical heterogeneity on the amount of acid injected as a function of injection rates. Liu et al. (2012) examined the effect of normally distributed porosities on wormholing patterns, and Zhang et al. (2014) studied wormhole propagation behavior and its effect of acid leakoff in acid fracturing with the two-scale model.

The two-scale models give a good prediction of the dissolution pattern for the fluid-mineral systems mentioned. They can also provide an estimation of the optimum injection rate for laboratory scale experiments but will require enormous computational power to be applicable for field scale simulation. For emulsified acid, the model does not account for emulsion droplet size distribution, and it is assumed that the droplets are very fine and will be unchanged as the acid propagates through the rock. For gelled acid, the

model does not account for polymer adsorption at the pore walls. First order irreversible reactions are assumed for the kinetics in these models, which makes them inapplicable for acidizing fluids with complex reaction kinetics with carbonates.

2.2. Analysis of the Outputs of Carbonate Matrix-Acidizing Models

The three main predictions of interest from an ideal acidizing model are the dissolution structure, optimum injection rate, and the wormhole propagation rate. The ability and accuracy of the existing models in literature to predict these outputs will be discussed in this section.

2.2.1. Dissolution Structure Prediction

The shape of the structure resulting from the dissolution of carbonate by the acidizing fluid determines the efficiency of the matrix treatment. Fig. 1.2 shows that the dominant wormhole structure is the most desired for optimum results (based on the least amount of acid required to achieve breakthrough), followed by conical or ramified wormhole patterns, and the least desirable structures for a successful treatment are the face or uniform dissolution of the rock.

Capillary tube approach models do not predict the various dissolution structures possible during carbonate acidizing. As the approach name implies, the shape of the wormhole is assumed to be cylindrical at model initialization. The models by Hung et al. (1989) and Huang et al. (1999) assume the overall reaction is mass transfer limited and that the acid is being injected at the optimum injection rate, with a dominant wormhole dissolution structure rigidly assumed. Buijse (2000) assumed a finite acid-rock reaction rate to account for mass transfer and mixed kinetics controlled reactions; dominant

wormhole structures exist if the reaction is solely mass transfer controlled and ramified wormholes exist in the case of mixed kinetics. Gdanski (1999) also models the dissolution structure as dominant wormholes with rigid assumptions on spatial distribution, the overall reaction in this model is assumed to be mass transfer controlled.

Transition pore theory based models do not predict the wormhole dissolution structure; these models only calculate the optimum injection rates. Semi-Empirical models (Buijse and Glasbergen 2005; Furui et al. 2012) also do not predict dissolution structures. Dominant wormholes are assumed for these models in calculating the propagation rate of the acid in the treated formation. Péclet number models only apply to mass transfer controlled systems, at and above the optimum injection rate (Fredd and Miller 2000). The model by Daccord et al. (1989) accounts for face dissolution, dominant wormholes, and ramified wormholes structures, and the Frick et al. (1994) model accounts for the dominant and ramified wormhole dissolution structures.

Network and Damköhler based models by Hoefner and Fogler (1988) and Fredd and Fogler (1998, 1999) account for all of the five possible dissolution patterns observed during carbonates acidizing based on the fluid-mineral system. The model by Fredd (2000) also predicts the dissolution structure. The shortcomings of these models have been highlighted in the literature review section.

Most of the recent two-scale models predict the dissolution structure. The model by Liu et al. (1997), which was originally developed for sandstones acidizing but can also model carbonate acidizing, only accounts for reaction rate controlled reactions; the model by Golfer et al. (2002) accounts only for dissolution in the mass transfer controlled regime.

Later models, initiated by Panga et al. (2004, 2005), account for dissolution in both the reaction rate and mass transfer controlled regimes; thus, they can predict any type of dissolution structure based on the fluid-mineral system.

2.2.2. Optimum Injection Rate Calculation

Coreflood experiments by various researchers have shown that the efficiency of a carbonate matrix acid treatment depends on the injection rate of the acidizing fluid and that there exists an optimum injection rate for any fluid-mineral system, as shown in Fig. 1.2. At the optimum injection rate, the least amount of acid propagates to form the most efficient dominant wormholes which penetrate deepest into the rock. Some of the carbonate matrix-acidizing models predict the optimum injection rates for coreflood experiments but the results do not translate accurately to field conditions mainly due to the effect of formation heterogeneities, scaling, and translation of linear flow in the laboratories to radial flow in the field.

Capillary-tube-based models do not predict the optimum injection rates for the most efficient treatment, models such as the ones developed by Hung et al. (1989), Gdanski (1999), and Huang et al. (1999) to calculate wormhole propagation assume the reaction is mass transfer controlled with the acid injected at or a bit above the optimum injection rate. Péclet number theory based models such as the ones by Daccord (1989) and Frick et al. (1994), and semi empirical based models such as the ones from Buijse and Glasbergen (2005) and Furui et al. (2012) do not predict optimum injection rate.

Models based on the Damköhler number, such as the transition pore theory models and the network models, predict the optimum injection rate for a fluid-mineral system.

Some averaged continuum models predict the optimum injection rate in the description of wormhole propagation also. The Damköhler number, N_{Da}, as presented by Fredd and Fogler (1998, 1999) is given by

$$N_{Da} = \frac{\pi d L \kappa}{Q}. \tag{2.1}$$

An optimum Damköhler number of 0.29 is obtained for all fluid-mineral systems investigated. The parameters d and L are diameter and length of the wormhole, respectively, q is the flow rate, and κ is the overall dissolution given by:

$$\kappa = \frac{1 + \frac{1}{\nu K_{eq}}}{\frac{1}{k_{cR}} + \frac{1}{\nu k_s} + \frac{1}{\nu K_{eq} k_{cP}}}, \tag{2.2}$$

where k_{cR} and k_{cP} are the mass transfer coefficients for reactants and products, respectively, k_s is the surface-reaction-rate constant, ν is the stoichiometric ratio of products to reactants, and K_{eq} is the reaction-equilibrium.

Models that use the Damköhler number theory are based on Eq. 2.1, from which the optimum flow rate is calculated, with the assumption that the optimum number of 0.29 applies for the particular fluid-mineral system being considered. An example is the transition pore theory model by Huang et al. (1997), which applies the Damköhler number as shown in Eq. 2.3:

$$u_{opt} = \frac{E_{f0} C_f^{m-1} exp\left(-\frac{\Delta E}{RT}\right)}{(N_{Da})_{opt}}. \tag{2.3}$$

The Damköhler number based model can be used to calculate the optimum injection rate for coreflood setups, but the results do not translate accurately for field

application. As discussed, network models are not available for practical application due to the large computational power required to translate to field or laboratory scale. For the transition pore theory based models, the optimum injection rate values obtained at high temperature conditions are not practical. According to Schechter (1992), the reaction rates are difficult to measure, and the rate law which is extrapolated from measurements taken at subzero temperatures may not be accurate under reservoir conditions. It is also noteworthy that the optimum Damköhler number of 0.29 for different fluid-mineral systems is obtained at room temperature in the laboratory and may not be applicable at high temperature at field conditions.

In the averaged continuum model by Panga et al. (2005), a qualitative criterion was developed, given by the parameter $\Lambda \sim O(1)$:

$$\Lambda = \frac{\sqrt{\varepsilon_o D_{eT} k_{eff}}}{u_o}. \tag{2.4}$$

The magnitude of the Λ parameter is used to determine the type of dissolution pattern. When $\Lambda << 1$, uniform dissolution occurs and when $\Lambda >> 1$ there is compact or face dissolution. Wormholes are formed when Λ is of order unity. ε_o is the initial porosity of the rock, D_{eT} is the effective transverse dispersion coefficient, and k_{eff} is similar to the overall dissolution coefficient defined in Eq. 2.5 and given by:

$$k_{eff} = \frac{1}{\frac{1}{k_s a_v} + \frac{1}{k_c a_v}}, \tag{2.5}$$

where k_s is the surface reaction rate constant, k_c is the pore-scale mass transfer coefficient, and a_v is the interfacial surface area, which are pore-scale properties dependent on the pore-structure of the rock.

The optimum injection velocity was approximated as follows:

$$u_{opt} \sim \sqrt{\left(\frac{k_c k_s}{k_s + k_c}\right) a_v D_{eT}} = \sqrt{k_{eff} D_{eT}}\,. \tag{2.6}$$

Another optimum injection rate model worth mentioning is the Gong and El-Rabaa (1999) model based on dimensionless parameters such as the Damköhler number, the Péclet number, and the acid capacity number. The equation for the optimum acid injection rate is given by:

$$q_{opt} = \frac{2.155}{k^{1/14}\left(\frac{\mu}{\rho}\right)^{2/7}} \left(\frac{ls\% \frac{c_1 k^{1/2} E_f D_{ls}^{5/3}}{C_o^{1-n}} + dl\% \frac{d_1 D_{dl}^{8/3}}{\mu_o^4}}{ls\% \frac{c_2}{\mu_o^{1/2}} \left(\frac{N_{ac}}{D^{1/3}}\right)_{ls} + dl\% \frac{d_2}{\mu_o^{-2}} \left(\frac{N_{ac}}{D^{1/3}}\right)_{dl}} \right)^{3/7} . \tag{2.7}$$

Apart from the constants c_1, c_2, d_1, and d_2 not being readily available to use for different rock types and acidizing fluids, calculation by Glasbergen et al. (2009) showed that the results from this model differed from that obtained experimentally by an order of magnitude.

2.2.3. Wormhole Propagation Rate Calculation

The wormhole propagation rate is an indicator of the efficiency of the acid treatment per volume of fluid injected. From the propagation rate, the skin evolution of the treatment is obtained using Hawkins' skin formula which gives an indication of the success of the treatment. The treatment is most efficient when dominant wormholes are

formed which penetrate deep into the formation, bypassing the damaged zone of the well being treated. Various models have been developed to calculate the wormhole propagation rate to monitor skin evolution during treatment. The assumptions in the development of these models and limitations in applicability for field conditions, if any, are discussed in this section.

The transition pore theory does not model wormhole propagation. Likewise, models primarily based on the Damköhler number do not calculate the wormhole propagation rate, but there are cases in which the Damköhler number approach is combined with another approach to model wormhole propagation. An example of such a model is that of the Damköhler number based model by Fredd (2000) in which wormholes are modeled by capillary tubes and the effects of the wormhole patterns on the radial and axial propagation rates are accounted for through the Damköhler number. Wormhole density and a wormhole fluid loss model are required to run this model. The network models also combine the Damköhler number and capillary tube approach, but this will not be discussed here due to the lack of practical application of network models and reported computational power limitations for laboratory and field scale translation.

The main purpose of models based on the capillary tube approach is to calculate the wormhole propagation rate. The model by Buijse (2000) does not provide the direct calculation of the wormhole propagation rate; it focuses more on the study of acid spending with tip splitting to understand the effect of the injection and diffusion rate on the wormhole propagation rate. The wormhole propagation model developed by Hung et al. (1989) is based on the wormhole being modeled as a cylindrical tube with fluid leakoff

along its wall. The authors assumed that the wormholes do not cross path as they propagate in the rock, and the actual reaction between the rock and acidizing fluid is instantaneous (the model only applies to mass transfer controlled systems). The acid concentration at the wormhole tip is also assumed to be equal to the acid concentration in the wellbore, and the viscosities of reservoir fluid and injection fluid are the same for the calculation of the fluid-loss rate. Like all capillary tube models, the microscopic pore distribution of the rock surface at which the acid is injected is required to initiate the model. The accuracy of this model depends on the pore-size distribution and the two methods to obtain this, shown by the authors, gave significantly different results.

The model by Gdanski (1999) is another capillary tube based model that only applies to mass transfer controlled systems. According to Fredd and Miller (2000), the initial conditions and assumptions of this model skew the results to incorrectly indicate that the length of the wormhole is not dependent on the injection rate and diffusivity. They also concluded that the output of this model is not consistent with most experimental observations because of the nature and number of the various assumptions made in the development of the model.

The Péclet number approach by Daccord et al. (1989), as previously explained, models wormhole propagation rate based on relationships between parameters and dimensionless numbers which are obtained from experiments and analytical considerations. The justification for the Péclet number dependence on the wormhole growth is erroneous and output on the effect of the diffusion coefficient are different from what was observed experimentally by Fredd and Miller (2000).

For the semi-empirical model approach, various experimental studies have shown that the optimum pore volume to breakthrough and the optimum injection velocity obtained from coreflood tests (which are used in the semi-empirical model) are dependent on the size of the core used. Furui et al. (2012) improved on the original semi-empirical model by Buijse and Glasbergen (2005) to account for the effects of core size used in the coreflood tests. The Furui et al. (2012) model combines the Buijse and Glasbergen model with the Hung et al. (1989) mechanistic model for wormhole propagation earlier described. The scale up technique developed by the authors extends linear coreflood tests to radial-flow observed in field applications, eliminating the core-size dependency and flow translation limitations.

The modified semi-empirical equation to calculate wormhole growth rate, v_{wh}, is given by Eq. 2.8:

$$v_{wh} = v_{i,tip} N_{ac} \times \left(\frac{v_{i,tip} PV_{bt,opt} N_{ac}}{v_{i,opt}} \right)^{-\gamma} \times \left\{ 1 - \exp\left[-4 \left(\frac{v_{i,tip} PV_{bt,opt} N_{ac} L_{core}}{v_{i,opt} r_{wh}} \right)^2 \right] \right\}^2 , \quad (2.8)$$

where $PV_{bt,opt}$ (pore volume to breakthrough at optimum injection velocity) and $v_{i,opt}$ (optimum interstitial velocity) are parameters obtained from laboratory coreflood tests. The acid capacity number (N_{ac}) is given by:

$$N_{ac} = \frac{\phi \alpha C_f \rho}{(1-\phi)\rho_s}. \quad (2.9)$$

For radial flow, the interstitial velocity ($v_{i,tip}$) is given by:

$$v_{i,tip} = \frac{Q}{\phi h \sqrt{\pi m_{wh}}} \left[(1-\alpha_z) \frac{1}{\sqrt{d_{e,wh} r_{wh}}} + \alpha_z \left(\frac{1}{d_{e,wh}} \right) \right]. \quad (2.10)$$

Spherical flow is given by the equation below:

$$v_{i,tip} = \frac{Q}{4\pi\phi d_{e,wh} r_{wh}}. \quad (2.11)$$

For radial flow, m_{wh} represents number of dominant wormholes along the angular direction, α_z denotes the wormhole axial spacing, and d_e is the effective diameter of the wormhole cluster.

2.3. Limitations of Carbonate Matrix-Acidizing Models for Field Application and Recommendations

Most of these models generally give good predictions of the optimal flow rate and/or wormhole growth rate for coreflood tests in the laboratory, but the model results do not translate properly for field conditions. Translation of linear flow in coreflood tests to radial flow under field conditions, formation heterogeneities, wormhole competition in field conditions, and effect of additives on the acidizing fluid dissolution rate are factors that limit the accuracy in the application of these models for field cases.

The benefit of acid stimulation is usually underestimated by theoretical and laboratory-based carbonate matrix-acidizing models because of their miscalculation of wormhole length and accompanying skin changes (Furui et al. 2012). A reason for this is that most of these acidizing models are based on coreflood tests in the laboratory, which are performed under linear flow conditions. Radial flow conditions are more common in field applications but are difficult to model in the laboratory. Another limiting factor in the application of existing matrix-acidizing models is the lack of representation in the acidizing models or coreflood tests when dealing with heterogeneous formations. The presence of vugs in carbonate formations, not accounted for in most of the existing acidizing models, will cause a change in the acidizing model-predicted flow rate and

pattern of the acidizing fluid. Heterogeneities in the permeability and porosity of the formation are also not properly accounted for in the design of most carbonate matrix-acidizing models, and this also affects the prediction of the optimum injection and wormhole propagation, especially for highly heterogeneous formations.

In extrapolating carbonate matrix-acidizing models or laboratory results to field scale, multiple wormholes need to be accounted for. Unlike in coreflood tests, there is formation of multiple wormholes in the field during an efficient acid treatment; this leads to wormhole competition for acidizing fluid and a different mechanism for fluid loss along the walls of the wormhole. The competition of wormholes for acidizing fluid in the field and the accompanying fluid loss effects will give different propagation rates than what is observed in the laboratory. To properly account for wormhole competition in matrix acidizing models, the wormhole density and the distribution of the dissolution structures have to be known. The accuracy in the methods to estimate these parameters to initiate wormhole propagation models for field cases is not reliable.

Existing matrix-acidizing models do not account for the effect of additives on the acidizing fluid. Experiments by Taylor et al. (2004) showed that different additives such as corrosion inhibitors, surfactants, mutual solvents, complexing agents, and polymers all have varying effects on the dissolution rate of acidizing fluid. Since it is not possible to perform an acid treatment procedure in the field without using additives, it is important to factor their effect on the dissolution rate of the acidizing fluid, which will determine the optimum injection rate and the propagation rate of the acid.

Due to the various highlighted limitations in translating the optimum injecting rate from linear coreflood experiments to radial field conditions and also the limitations of the matrix acidizing models based on these experiments, the accurate method to determine the optimum injection rate for field applications is still uncertain. A suitable model will be the modified transition pore theory by Huang et al. (1997), as presented in Eq. 2.3, but the kinetic parameters to obtain an accurate optimum injection rate prediction at high temperature conditions are not available at this time.

Coreflood tests have shown that it is better to inject above the experimentally determined optimum injection rate than below it. Therefore it is recommended that the acidizing fluid should be injected at the maximum allowable injection rate for field application. The maximum allowable injection rate is based on the fracture pressure limit of the reservoir and can be calculated from inflow performance relationships with pseudo steady-state conditions.

Maximum allowable injection rate for vertical wells (Economides et al. 1994):

$$Q_{max} = \frac{kh(p_f - \bar{p})}{141.2\mu\left[\left(\ln\frac{0.472r_e}{r_w}\right) + S\right]}, \tag{2.12}$$

where p_f is the fracture pressure and $\bar{p}$ is the reservoir pressure.

Maximum allowable injection rate in horizontal wells (Economides et al. 1991):

$$Q_{max} = \frac{7.08 \times 10^{-3} L_h k(p_f - \bar{p})}{\mu\left\{0.5\ln\left[\left(\frac{8hI_{ani}}{\pi r_w(I_{ani}+1)}\right)\cot\left(\frac{\pi z_w}{2h}\right)\right] + 0.5\left[s - \frac{(h - z_w)I_{ani}}{L}\right]\right\}}, \tag{2.13}$$

$$k = \sqrt{k_H k_V}, \tag{2.14}$$

and

$$I_{ani} = \sqrt{\frac{k_H}{k_V}}, \tag{2.15}$$

where I_{ani} is the measure of horizontal to vertical permeability and z_w is the elevation of the well from the reservoir bottom. . **Fig. 2.1** depicts the representation of the horizontal well model as originally developed by Kuchuk et al. (1990).

To monitor skin evolution during the matrix acidizing treatments, the wormhole propagation can be calculated using the semi-empirical model developed by Furui et al. (2012). This model accounts for the core-size dependencies in the translation of laboratory coreflood results to field application and also the radial flow typically observed in field application. This model does not completely eradicate all the highlighted limitations, but it is the most practically applicable one in theory. It is assumed in the application of this model that the overall reaction is mass transfer controlled or mixed kinetics. The additive that is used in the field for the treatment should also be used with the acidizing fluid in the laboratory experiments when the optimum flow rate parameters are obtained during coreflood tests.

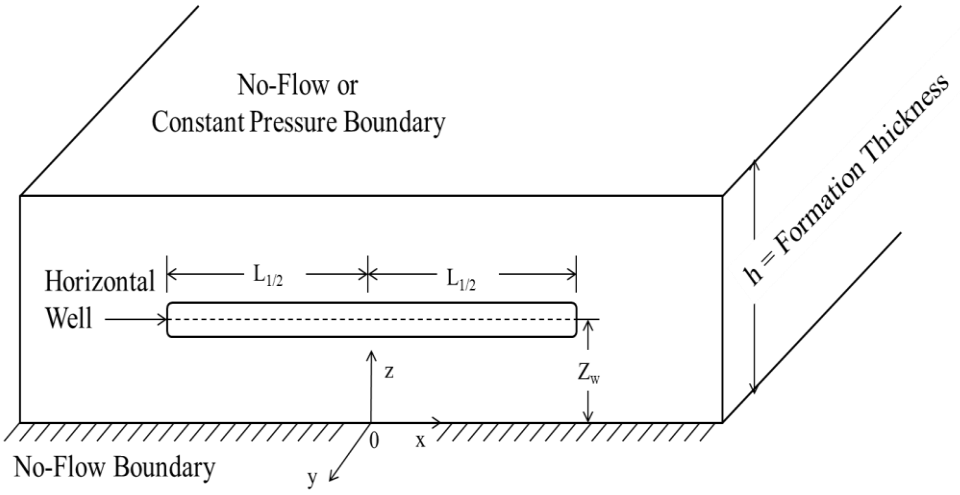

Fig. 2.1–Horizontal well model (reprinted with permission from Kuchuk et al. 1990).

2.4. Section Conclusions

The carbonate matrix acidizing models in the literature have been analyzed in this section to make the following conclusions:

1. Most of the available carbonate matrix-acidizing models are fairly accurate in their predictions of the dissolution structure, optimum injection, and/or wormhole propagation rates for coreflood tests in the laboratory.
2. The accuracy in the application of available carbonate matrix-acidizing models for field cases is hindered by factors such as translation of linear flow in coreflood to radial flow under field conditions, formation heterogeneities, wormhole competition in field conditions, and the effect of additives on acidizing fluid dissolution rate.

3. It is recommended to inject the acidizing fluid at maximum allowable injection rates (from calculations based on the fracture pressure limits) for a carbonate matrix acidizing treatment in the field.
4. The modified semi-empirical wormhole propagation model is recommended in field application for the calculation of wormhole growth rate for skin evolution during treatment.
5. The effect of additives on the dissolution rate of the acidizing fluid should be considered in the application of any carbonate matrix acidizing model for field cases.

3 TWO-SCALE MODEL WITH NAVIER-STOKES MOMENTUM FORMULATION

3.1. Introduction

The two-scale model approach offers the most accurate method to investigate and increase the understanding of wormhole propagation during carbonate matrix acidizing. The approach provides the best model to predict optimum injection and wormhole propagation rates at the laboratory scale, but will require massive computational power to translate to large field scale, which is why it was not recommended for direct practical field application in the previous section.

In this section, the two-scale model is modified with the fluid flow field described by the Navier-Stokes momentum formulation. This formulation reduces the computational time of numerical simulation at high injection rates compared to previously used Darcy and Darcy-Brinkman formulations. The model is implemented using FLUENT^{TM} (ANSYS FLUENT 15.0), a commercial computational fluid dynamics package, to solve the momentum and transport equations in the Darcy scale. The software is combined with functions and routines written in the C programming language to solve the porosity evolution equation, update the pore scale parameters at every time step in the simulation, and couple the Darcy and pore scales.

3.2. Model Description

A detailed description of the development of the two-scale model is presented in Panga et al. (2002, 2005). The flow field is described by Darcy's law in their model, but

in the present study the flow field is described by the Navier-Stokes momentum formulation. The equations for the Darcy and pore scale models are presented below:

3.2.1. Darcy Scale Equations

The fluid flow field is given by the Navier-Stokes formulation:

$$\frac{\partial(\rho\mathbf{u})}{\partial t} + \nabla\cdot(\rho\mathbf{u}\mathbf{u}) = -\nabla p + \nabla\cdot\boldsymbol{\tau} - \frac{\mu}{\mathbf{K}}\mathbf{u}, \tag{3.1}$$

where **u** is the superficial velocity vector, ρ is the fluid density, **K** is the permeability tensor, p is pressure, and $\boldsymbol{\tau}$ is the stress tensor. The continuity, Eq. 2, derived from the mass balance of fluids, accounts for the effect of local volume change during dissolution on the flow field:

$$\frac{\partial\varepsilon}{\partial t} + \nabla\cdot\mathbf{u} = 0. \tag{3.2}$$

The Darcy scale description of the transport of acid species, from fluid phase balance of reacting species, is given by

$$\varepsilon\frac{\partial C_f}{\partial t} + \mathbf{u}.\nabla C_f = \nabla\cdot\left(\varepsilon\boldsymbol{D_e}\cdot\nabla C_f\right) - k_c a_v\left(C_f - C_s\right), \tag{3.3}$$

where ε is the porosity of the medium, C_f is original concentration of the acid in the fluid phase, C_s is the concentration of the acid at the fluid-solid interface, $\boldsymbol{D_e}$ is the effective dispersion tensor, k_c is the local mass-transfer coefficient, and a_v is the interfacial area available for reaction per unit volume of the medium. The reaction kinetics in Eq. 3.4 balances the amount of acid transferred from the fluid phase to the surface to the amount reacted at the surface:

$$k_c\left(C_f - C_s\right) = R(C_s). \tag{3.4}$$

The porosity evolution equation, derived from the balance between the solid dissolved and fluid consumed, is given by:

$$\frac{\partial \varepsilon}{\partial t} = \frac{R(C_s) a_v \alpha}{\rho_s}, \tag{3.5}$$

where R (C_s) represents the reaction kinetics, ρ_s is the density of the rock, and α is the dissolving power of the acid. Equations 3.1 through 3.5 are the Darcy scale model equations, as described by Panga et al. (2005). For a first order reaction, the kinetics equation is expressed as $R(C) = k_s C_s$ (where k_s is the dissolution rate constant), and then Eq. 3.4 is modified to:

$$C_s = \frac{C_f}{\left(1 + \frac{k_s}{k_c}\right)}. \tag{3.6}$$

3.2.2. Pore Scale Equations

The porosity of the rock increases as the acid propagates and dissolves part of the solid phase. This results in changes of pore-scale properties such as permeability, pore-radius (r_p), and interfacial surface area per unit volume. The relationship between these rock properties and porosity are adapted from the Carman-Kozeny correlation and are given by the following pore scale equations (Panga et al. 2005):

$$\frac{\boldsymbol{K}}{\boldsymbol{K}_o} = \frac{\varepsilon}{\varepsilon_o}\left(\frac{\varepsilon(1-\varepsilon_o)}{\varepsilon_o(1-\varepsilon)}\right)^{2\beta}, \tag{3.7}$$

$$\frac{\boldsymbol{r_p}}{\boldsymbol{r_o}} = \left(\frac{\varepsilon(1-\varepsilon_o)}{\varepsilon_o(1-\varepsilon)}\right)^{\beta}, \tag{3.8}$$

and

$$\frac{\boldsymbol{a_v}}{\boldsymbol{a_o}} = \left(\frac{\varepsilon}{\varepsilon_o}\right)\left(\frac{\varepsilon(1-\varepsilon_o)}{\varepsilon_o(1-\varepsilon)}\right)^{-\beta}, \tag{3.9}$$

where β is the pore structure relation constant. The local mass transfer and effective dispersion coefficients are obtained using the following correlations (Gupta and Balakotaiah 2001; Balakotaiah and West 2002):

$$Sh = \frac{2\boldsymbol{k_c}r}{D_m} = Sh_\infty + 0.7Re_p^{1/2}Sc^{1/3}, \tag{3.10}$$

$$\boldsymbol{D_{eX}} = \alpha_{os}D_m + \frac{2\lambda_X\|\mathbf{u}\|r}{\varepsilon}, \tag{3.11}$$

and

$$\boldsymbol{D_{eT}} = \alpha_{os}D_m + \frac{2\lambda_T\|\mathbf{u}\|r}{\varepsilon}, \tag{3.12}$$

where *Sh* is the Sherwood number or dimensionless mass-transfer coefficient; Sh_∞ is the asymptotic Sherwood number; Re_p is the Reynolds number defined by $\mathrm{Re}_p = \frac{2\|\mathrm{u}\|r}{v}$, and *Sc* is the Schmidt number given by $Sc = \frac{v}{D_m}$; *v* is the kinematic viscosity; α_{os} is a constant that depends on the structure of the porous medium (pore connectivity); D_{eX} is the longitudinal dispersion coefficient; D_{eT} is the longitudinal dispersion coefficient in the y- and z- directions; λ_X and λ_T are constants that depend on the structure of the medium ($\lambda_X \approx 0.5$ and $\lambda_T \approx 0.1$ for a packed bed of spheres). These correlations account for both diffusive and convective contributions (Maheshwari and Balakotaiah 2013).

3.2.3. Flow Field Description

In the Liu et al. (1997) and Golfier (2002) averaged-continuum models, the fluid flow field was described by the Darcy-Brinkman formulation in order to accurately predict

the flow field when the Reynolds number is greater than one and the viscous contribution to the flow is significant (Panga et al. 2002). The flow in both the porous media and fluid (wormholes and vugs) is represented in this formulation. However, various investigators have shown that Darcy's law can be used to effectively describe fluid flow in the two-scale model and is computationally less expensive than the Darcy-Brinkman formulation.

In the two-scale model used in this study, the fluid flow is described by the Navier-Stokes formulation. This formulation was used by De Oliveira et al. (2012) in their two-scale model to study the effect of mineralogical heterogeneity on wormhole patterns, but the dissolution regimes at very low injection rates were not presented in their work. Like Darcy-Brinkman, the Navier-Stokes formulation allows a natural transition between flow in porous media and fluid (wormholes and vugs) and is also computationally less expensive than the Darcy-Brinkman formulation. Also, the computational time required in the ramified and uniform dissolution regime is considerably reduced using the Navier-Stokes formulation compared with Darcy's law based formulation.

3.3. Model Implementation

To run the simulations of the described two-scale model with Navier-Stokes formulation, FLUENT is employed to solve the momentum, mass continuity, and transport equations in the Darcy scale. This is combined with functions and routines written in the C programming language to solve the porosity evolution equation, update the pore scale parameters at every time step, and couple pore scale with the Darcy scale. The workflow of the simulation showing the sequence of equations solved in the model is illustrated in **Fig. 3.1**.

The simulations are run on the Texas A&M University (TAMU) High Performance Research Computing (HPRC) facility to enhance parallel processing. In the dominant wormholing regime, the computational time is nearly 3 to 4 hours, but the time taken to achieve breakthrough in the ramified and uniform dissolution regimes (high injection rates) is lower than that. At very low injection rates (face dissolution regime), the computational time is in days.

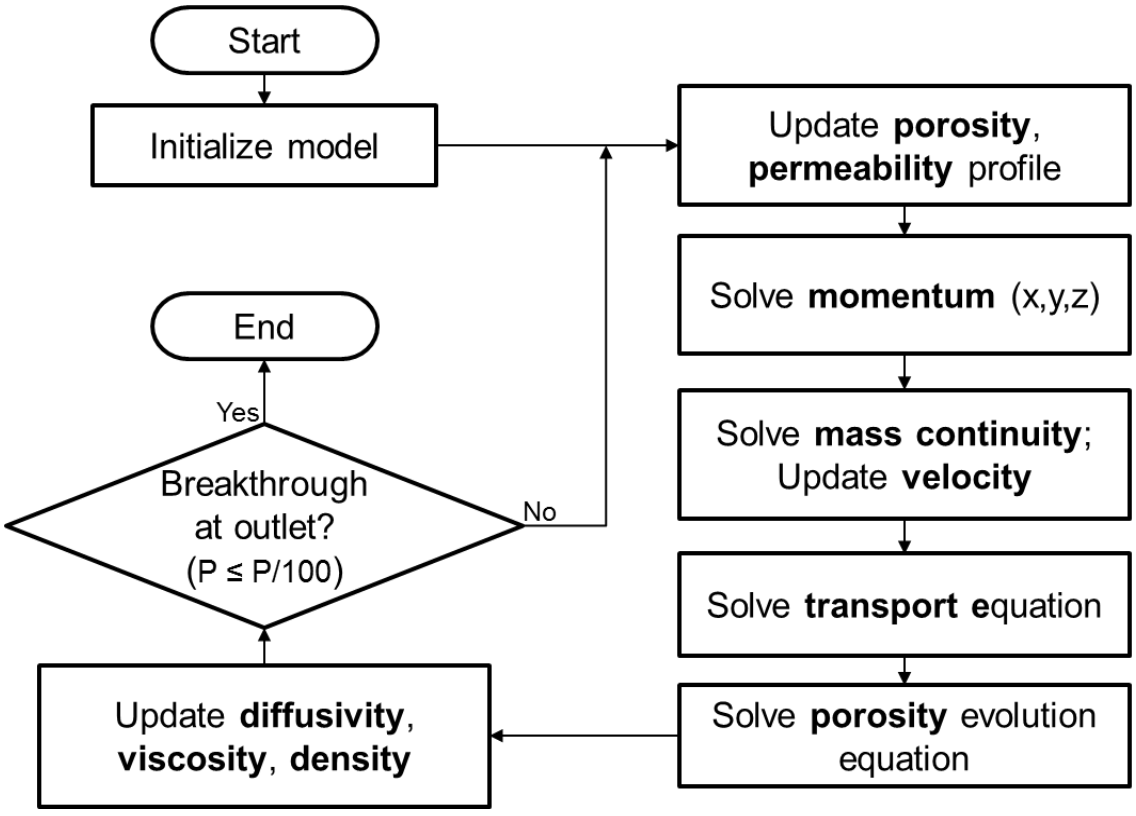

Fig. 3.1–The simulation workflow showing the sequence of solutions and properties updates.

3.3.1. Base Case

The base case is modeled to simulate the acidizing coreflood tests of 0.5 M HCl on limestone core samples, based on the experimental work by Fredd and Fogler (1998). In the simulation study for the 3D model, the numerical mesh domain is a 4 in. long cylindrical shape with a 1.5 in. diameter. The grid cells are made of 400,000 hexahedral and quadrilateral cells. For the 2D case, the numerical mesh domain is rectangular with a dimension of 1.5×4 in. and made up of 110,000 quadrilateral grid cells. The values of the parameters used in the base case of this simulation study are presented in **Table 3.1**. The values are obtained from the aforementioned experimental work of Fredd and Fogler (1998) and simulation study by Maheshwari and Balakotaiah (2013). The experiments were conducted at temperature of 23°C.

At very low rates (face dissolution regime), the number of grid cells has to be increased to effectively capture the dissolution at these regimes. According to Maheshwari and Balakotaiah (2013), approximately 160 million grid cells will be required to effectively capture face dissolution for the mesh domain size of a 1.5×1.5×4 in. rectangular parallelepiped domain, which is similar to the cylindrical domain of 1.5 in. diameter by 4 in. length used in this study.

As expected, more computational time will be required to complete the simulation at very low injection rates because the dissolution takes place at a slower rate and more of the carbonate rock will be dissolved in the face dissolution regime. In addition, since a high number of grid cells are required to accurately capture the dissolution pattern at these regimes, the simulation runs at a much slower rate in real time, which means more

computational time will be needed. Unfortunately, there are limited high performance computing licenses available for FLUENT parallel computing at the TAMU HPRC facility to practically run simulations at face dissolution regimes for this large computational mesh domain and high number of grid cells.

Parameter	Value
Acid diffusivity (D_m)	3.6e-09 m^2/s
Acid dissolving power (α)	50 kg/kmol
Acid viscosity (μ)	0.001 kg/m-s
Asymptotic Sherwood number (Sh_∞)	3.66
Average porosity (ε_o)	0.2
Constant in dispersion correlations (α_{os})	0.5
Constant in axial dispersion correlation (λ_x)	0.5
Constant in transverse dispersion correlation (λ_T)	0.1
Initial average permeability (K_o)	1e-15 m^2
Initial interfacial area per unit volume (a_o)	5000 m^{-1}
Initial mean pore size (r_o)	1 μm
Pore structure relation constant (β)	1
Porosity heterogeneity magnitude ($\Delta\varepsilon_o$)	± 0.1
Rock density (ρ_s)	2710 kg/m^3
Surface dissolution reaction-rate constant (k_s)	0.002 m/s

Table 3.1–Values of parameters used in numerical simulations.

The current solution to this limitation is to use a smaller mesh domain to capture and demonstrate the dissolution patterns at the conical and face dissolution regimes. The domain is reduced by a factor of 5 for the 3D and 2D linear cases with the number of grid

cells kept the same. The pore volumes to breakthrough (PV_{BT}) results for the larger domain compare qualitatively with that of the smaller domain at and above the optimum injected rates, and this is extended for rates below the optimum injection rate. Information on other domain sizes used in this work to study the radial flow and the effect of medium dimensions on the acid efficiency curve will be provided in the discussion of results.

3.3.2. Numerical Solution Scheme

A control-volume-based technique is used to solve the momentum conservation and transport equations in the Darcy scale of the two-scale model. The equations are converted to algebraic equations which are then solved numerically with the finite volume method.

A Pressure-Implicit with Splitting of Operators (PISO) pressure-velocity coupling scheme is employed, with neighbor and skewness correction to improve efficiency. A least squares cell based spatial discretization method is used for constructing the fluid concentration values at the cell faces with a second order upwind scheme, and a Quadratic Upstream Interpolation for Convective Kinematics (QUICK) scheme is used for the momentum term.

The time step size for the numerical simulation is varied between 0.1s and 0.01s, depending on the dissolution regime. The lower time step size is used at the conical and face dissolution regimes. The maximum number of iterations per time step is set at 20.

3.3.3. Initial and Boundary Conditions

For wormholes to be initiated in the carbonate rock, there must be some heterogeneity in the porous medium. This is introduced in this model in the form of

porosity heterogeneity. The average porosity of the base case is 0.2 with a heterogeneity of 50%, which means the values in the porosity distribution profile range from 0.1 to 0.3. A least squares interpolation method is then used to assign the porosity values from the generated profile to individual grid cells in the numerical domain. **Fig. 3.2** shows the initial porosity distribution for the different domain cases used in this study. Other initial conditions are zero velocity field in the medium and zero acid concentration.

The boundary condition at the core inlet is a constant injection velocity, based on the input for the particular simulation run, and a concentration of 0.5 M HCl. At the core outlet, the acid flux and the pressure are set to zero. There is no flow and zero acid flux across the boundary at the walls of the domain.

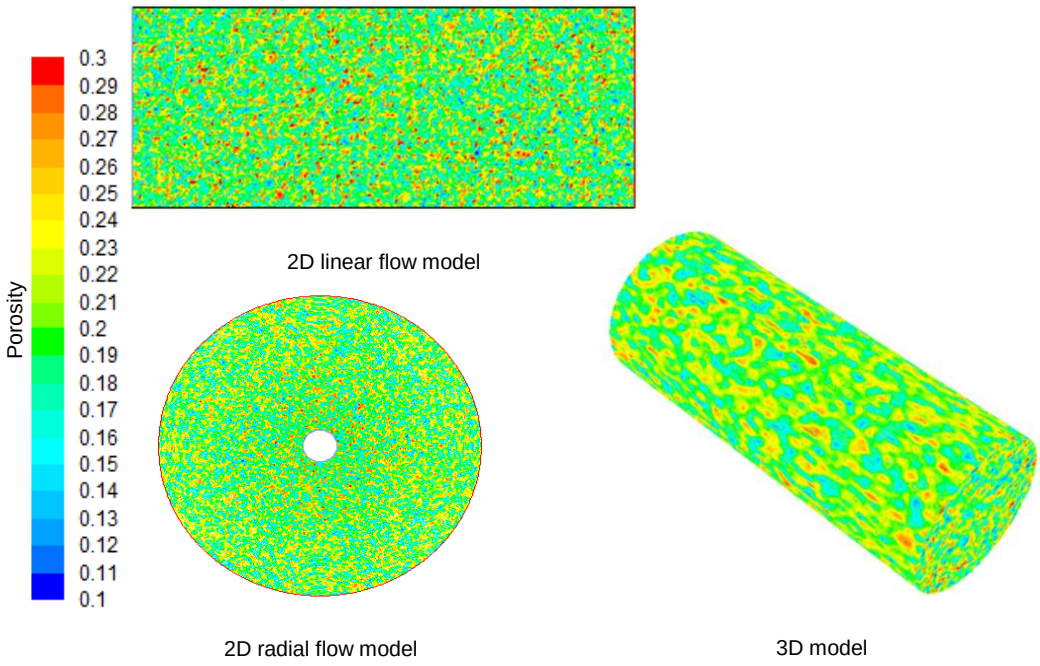

Fig. 3.2–The initial porosity profile of domain cases used in this study.

4 STUDY OF WORMHOLE PROPAGATION WITH THE TWO-SCALE MODEL

4.1. Introduction

This section explores the propagation of wormholes during carbonate matrix acidizing with the developed two-scale model while simultaneously performing sensitivity tests on this model and comparing the output with previous models and reported experimental results.

The results of most of the simulation carried out in this study are presented mainly in the form of acid efficiency curves. This is a plot of the PV_{BT} versus the injection rate or velocity. From these curves, the optimum injection rate and the minimum PV_{BT} values for the conditions being investigated can be observed. The breakthrough time of acid at the outlet of the core in the numerical simulation is determined to be when the pressure drop across the porous medium drops to 1/100th of its initial value (Kalia and Balakotaiah 2009).

4.2. 2D and 3D Linear Flow Model

The results from the 2D and 3D flow models are presented here. The dissolution patterns from a 2D simulation model with linear flow are displayed in **Fig. 4.1** by the porosity contour of the numerical simulation of the coreflood acidizing process. The output shows that the model effectively captures the dissolution patterns in carbonate acidizing and also shows the effect of injection rate (and Damköhler number) on the type of dissolution pattern formed.

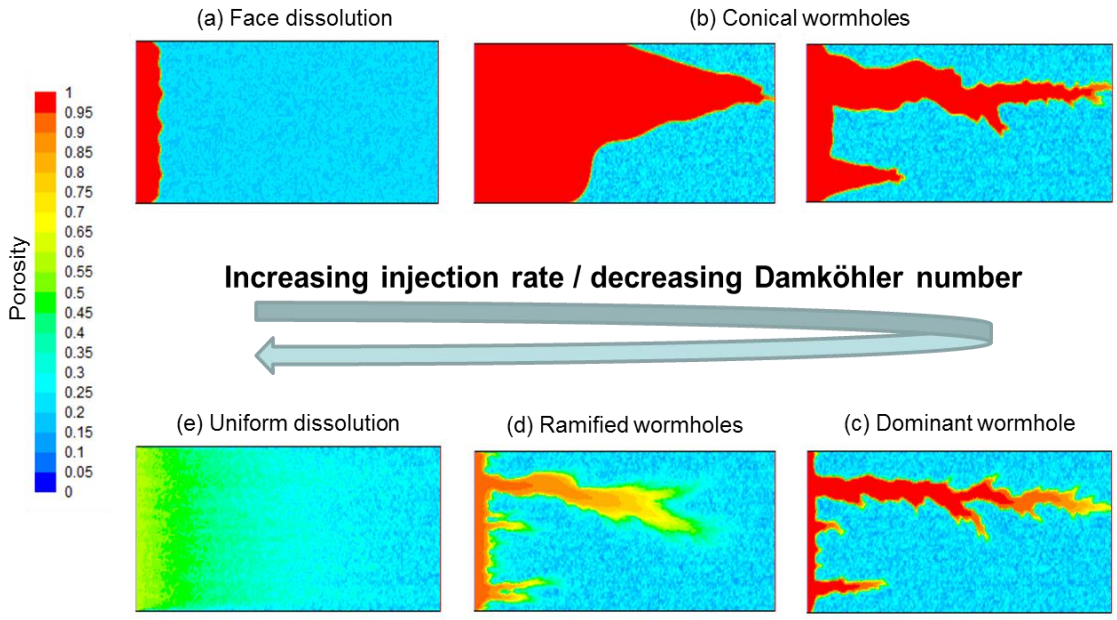

Fig. 4.1–Porosity contour showing the dissolution patterns obtained at various injection rates from the 2D linear flow model.

The acid efficiency curve from the 2D linear flow model is presented in **Fig. 4.2**. The semi-log plot of the acid efficiency curve above shows that at low injection rates, a large amount of acid is required to reach breakthrough at the outlet of the porous medium. This is because face dissolution occurs at these rates and the acid will have to completely dissolve the solid phase before fluid breakthrough is observed at the exit of the core. The amount of acid to breakthrough decreases as the injection rate increases until it reaches an optimum injection rate at which minimum PV_{BT} occurs. The amount of acid required to breakthrough gradually increases at rates above the optimum injection rate.

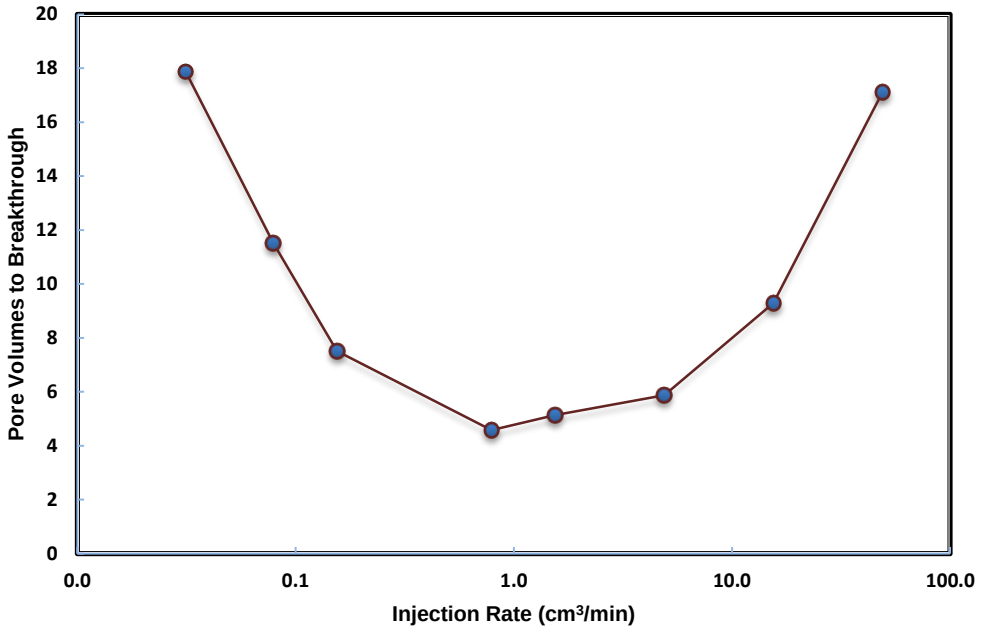

Fig. 4.2–The acid efficiency curve of the 2D numerical simulation with linear flow showing the effect of the injection rate on the amount of acid required to achieve breakthrough.

The PV_{BT} is observed to increase with the acid injection rate (Q) as $Q^{1/3}$, which is similar to the experimental results reported by Frick et al. (1994) and Bazin (2001). At very high injection rates (in the uniform dissolution regime), the slope of the plot is observed to change from one-third to unity. This trend of the proportionality of the acid injection rate and PV_{BT} values above optimum injection rate was also reported by simulation studies conducted by Maheshwari and Balakotaiah (2013).

The output from the numerical simulation of the 3D linear flow model showing the various dissolution regimes are presented in **Fig. 4.3** and the patterns are similar to experimentally observed dissolution images reported in previous studies (Hoefner and Fogler 1988; Fredd and Fogler 1998; Fredd and Miller 2000). The dissolution process and

the effect of injection rate on wormhole formation in the 3D model are similar to those in the 2D model, as explained in the previous section.

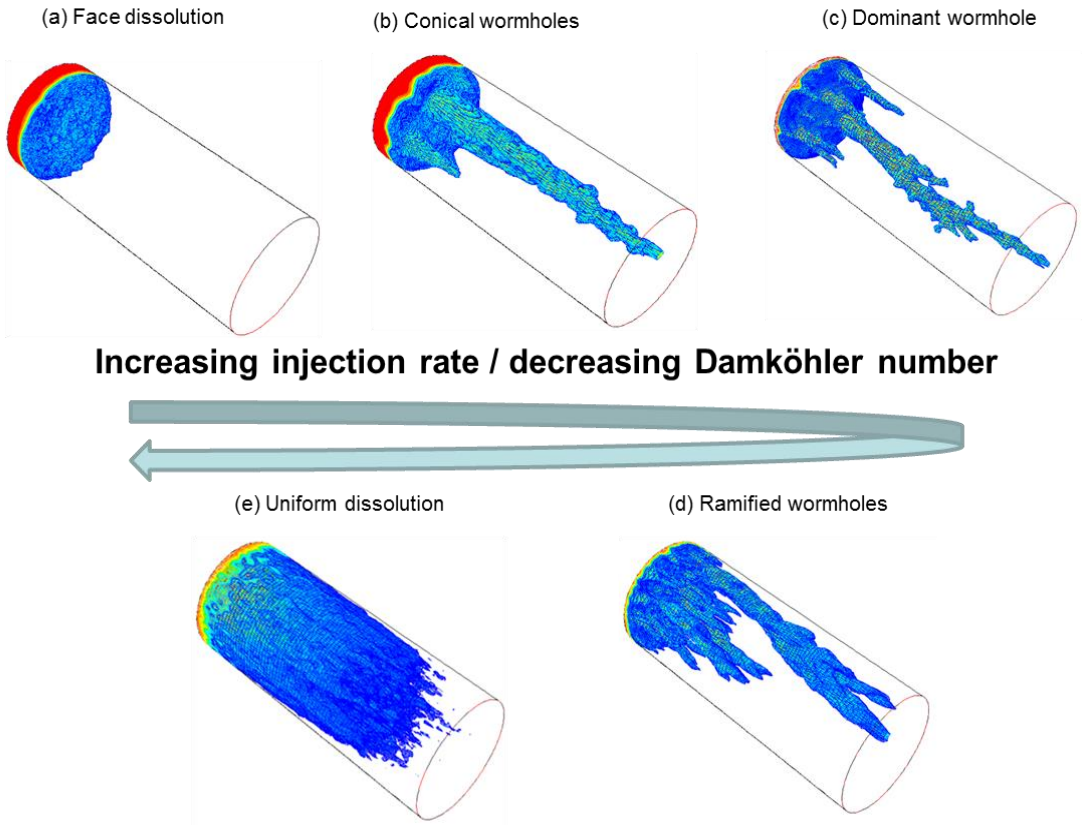

Fig. 4.3–Dissolution patterns from the numerical simulation of the 3D linear flow model.

The comparison of the acid efficiency curves from the 2D and 3D models is presented in **Fig. 4.4**. The compared output from this study follows the expected qualitative trend in a previous study (Panga et al. 2005). The plot shows that the amount of acid required to breakthrough in the wormhole regimes and the optimum injection rate

are higher in the 2D than in the 3D model. The difference in PV_{BT} values is because in 2D, the wormhole volume is the wormhole surface in two discretized directions multiplied by the depth of the domain in the third undiscretized direction, and this volume is greater than the wormhole volume in the 3D model (Cohen et al. 2008). The PV_{BT} values at the face and uniform dissolution regimes are independent on the dimension of the model because spatial gradients do not appear in the asymptotic limits (Panga et al. 2005).

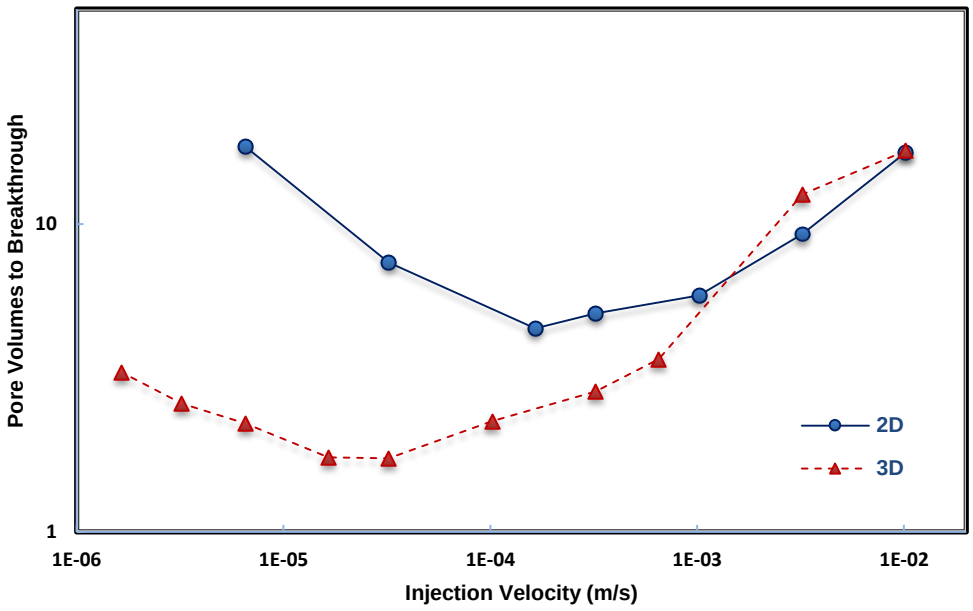

Fig. 4.4–Comparison of the acid efficiency curves from the numerical simulation of 2D and 3D models

4.3. 2D Radial Flow Model and the Effect of Flow Geometry.

To investigate the effect of flow geometry on the acid efficiency curve, a 2D radial flow model is developed for comparison with the 2D linear flow model having the same

aspect ratio. The 2D domain is a circular mesh with an external radius of 0.79 inches and an internal radius of 0.079 inches. The mesh is made up of 110,000 quadrilateral grid cells. The acid injection inlet is at the internal radius, and the fluid propagates radially towards the external radius until breakthrough is observed at the boundary. The dissolution patterns from radial flow are similar to the patterns from the linear flow model (**Fig. 4.5**).

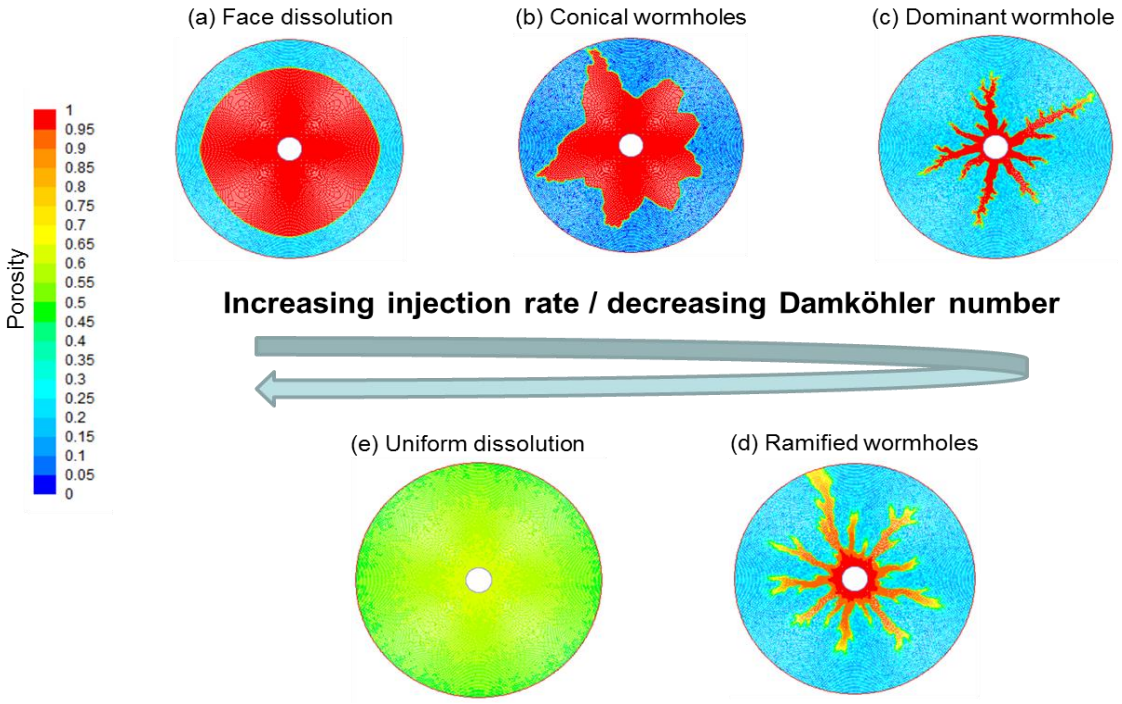

Fig. 4.5–Porosity contour showing the dissolution patterns obtained at various injection rates from the 2D radial flow model.

Fig. 4.6 shows the comparison of the acid efficiency curves from the radial and linear flow models. The optimum injection rate in the radial flow model is higher than that

of linear flow. The optimum injection rate in the radial flow model is higher because the injection velocity decreases with the increasing domain radius as the wormholes propagate in the medium (Kalia and Glasbergen 2009). There is enhanced branching of wormholes in the radial flow model, and these wormholes are thinner than those in the linear flow model. Thus, the PV_{BT} at the optimum injection rate in the radial flow model is lower than that of the linear model. These results are consistent with observations from previous studies (Frick et al. 1994; Cohen et al. 2008).

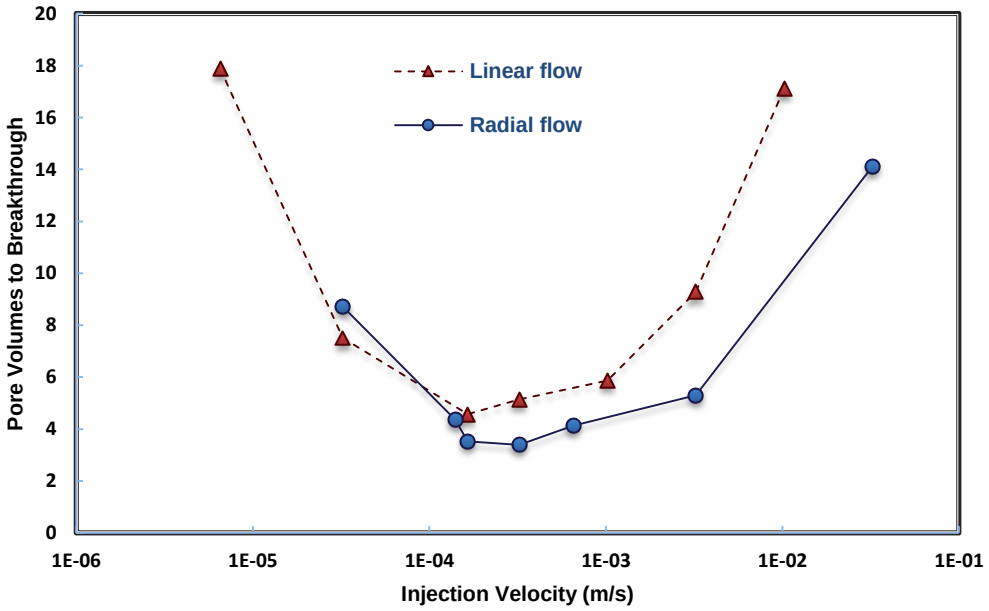

Fig. 4.6–The comparison of the acid efficiency curve of the linear and radial flow 2D cases show that the optimum injection rate is higher for the radial case with lower amount of acid required to achieve breakthrough.

4.4. Effect of Initial Average Porosity

To study the effect of initial average porosity on wormhole propagation, three 2D linear flow cases of initial average porosity values of 0.1, 0.2, and 0.3 with the same porosity heterogeneity range of 50%, are simulated. **Fig. 4.7** shows the dissolution patterns at the optimum injection rate. The higher the initial average porosity of the medium, the larger the wormhole diameter due to more fluid loss along the walls of the wormhole. **Fig. 4.8** shows the acid efficiency curves highlighting the amount of acid injected to breakthrough for the three cases.

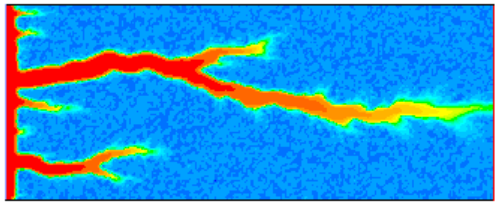

(a) $\varepsilon_o = 0.1$

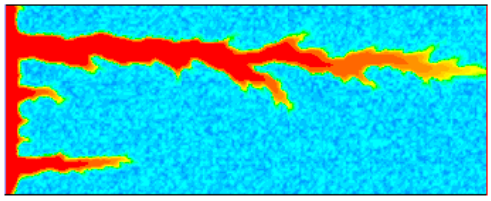

(b) $\varepsilon_o = 0.2$

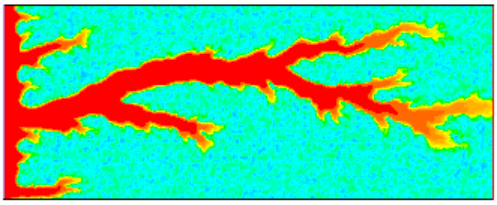

(c) $\varepsilon_o = 0.3$

Fig. 4.7–Effect of initial average porosity on wormhole dissolution patterns.

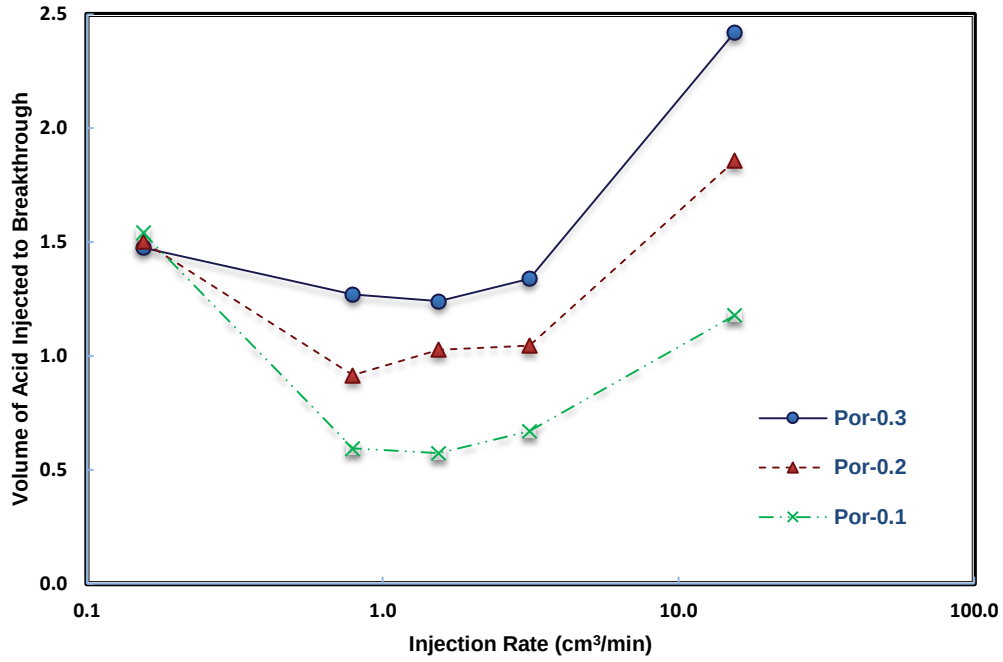

Fig. 4.8–Acid efficiency curves showing the effect of initial average porosity on the total volume of acid injected.

In the face dissolution regime, a higher amount of acid is required to breakthrough for cases with lower initial average porosity values. This is because complete dissolution of the rock occurs in this regime, and the lowest porosity case will require the most amount of acid to achieve breakthrough due to the highest percentage of solid phase in the medium. In the intermediate regime, the acid injected to breakthrough is higher for cases with higher initial average porosity because of the formation of wider wormholes, as previously explained. At high injection rates, there is increased fluid loss in the medium for cases with high initial porosity, requiring more acid to achieve a certain factor of increase in permeability than for low initial porosity cases.

4.5. Effect of Porosity Heterogeneity

The influence of medium heterogeneity on wormholing and PV_{BT} is examined here. Cases with porosity heterogeneity ranging from 0.5% to 0.95% of average porosity are simulated. It can be seen that the wormholes become thinner and more branched as the heterogeneity of the medium increases (**Fig. 4.9**). The acid efficiency curves of the various cases simulated with different heterogeneity magnitude values are shown in **Fig. 4.10**, and the effect of heterogeneity magnitude on PV_{BT} at the optimum injection rate is presented in **Fig. 4.11**.

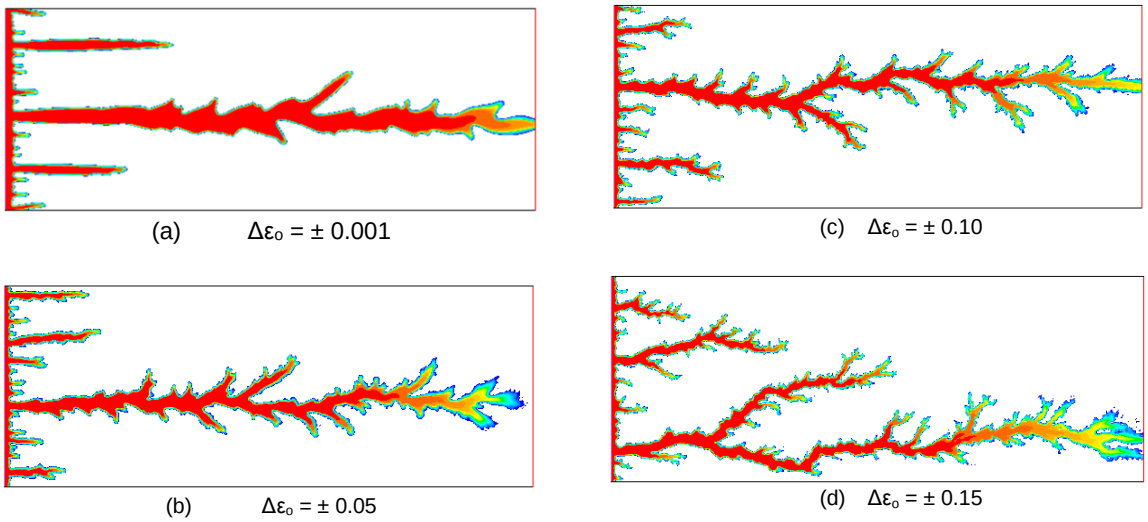

Fig. 4.9–Dissolution structures showing the effect of porosity heterogeneity magnitude on the wormhole patterns.

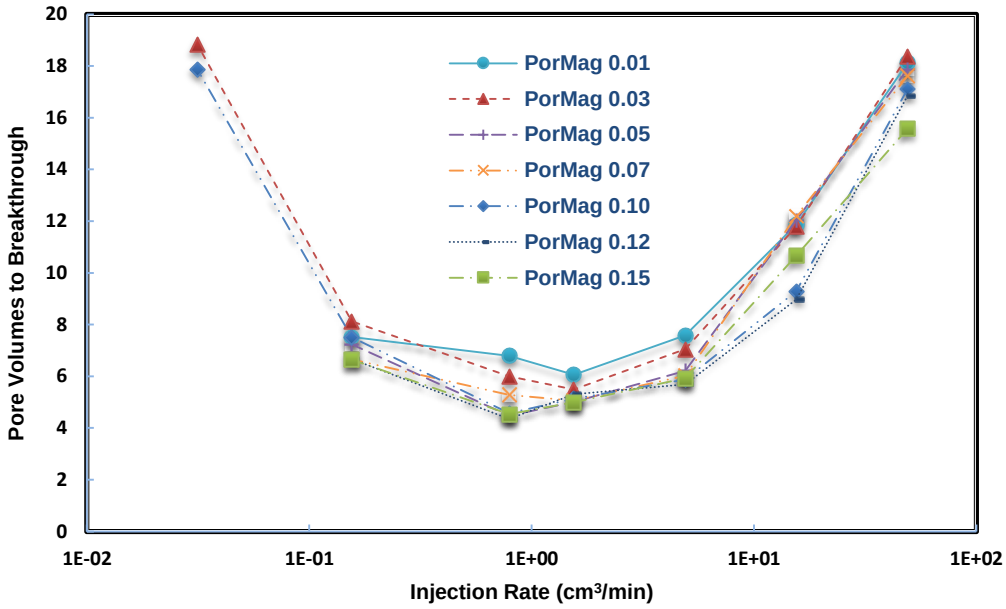

Fig. 4.10–Acid efficiency curves showing the effect of porosity heterogeneity magnitude on the pore volumes of acid required to achieve breakthrough.

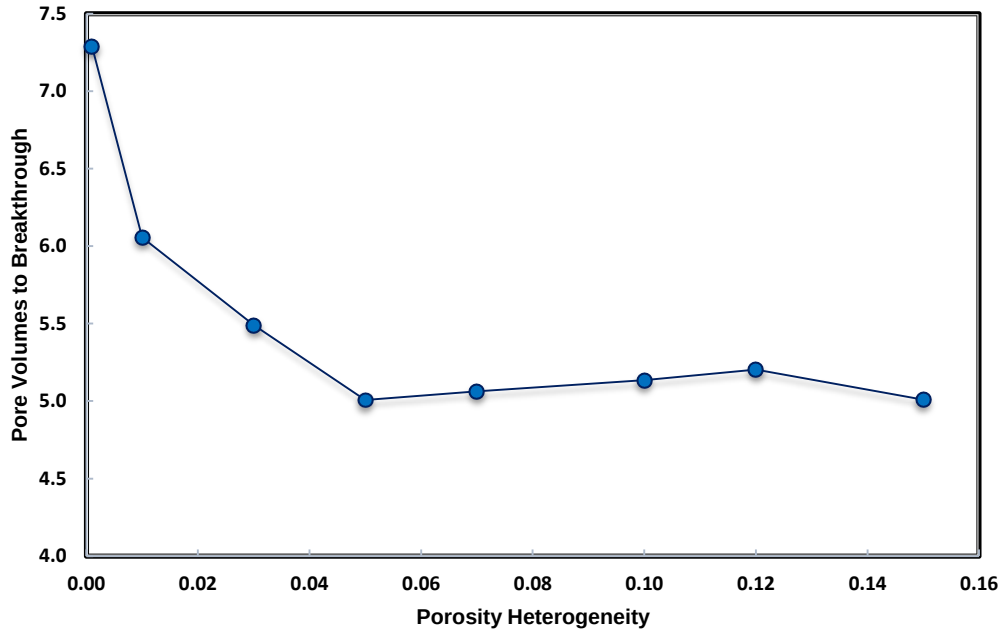

Fig. 4.11–Effect of porosity heterogeneity on PV_{BT} at the optimum injection rate.

The difference in the PV_{BT} values for the various heterogeneity cases is pronounced in the wormholing regime, but not as much as in the face and uniform dissolution regime (Fig. 4.10). In the uniform dissolution regime, the PV_{BT} slowly decreases as the porosity heterogeneity magnitude increases. This is because at a high heterogeneity magnitude, ramified wormholes tend to form (instead of uniform dissolution) more than they would at a lower heterogeneity magnitude with the same injection rate, which leads to a reduced amount of acid required for breakthrough.

At the optimum injection rate, Fig. 4.11 shows that the PV_{BT} will be high for cases with very low heterogeneity magnitude. This is because for a rock with very low heterogeneity, the dissolution process resembles that of face dissolution at the initial stage before branching occurs and an additional amount of acid will be consumed in the dissolution of the face of the rock (Fig. 4.9a). Another reason for high PV_{BT} values for cases with low heterogeneity magnitude is that the diameter of the wormholes is thicker and less branched, also requiring more acid for propagation.

It is also observed that PV_{BT} decreases with an increase in porosity heterogeneity magnitude (Fig. 4.11) until a critical value ($\Delta\varepsilon_c = \pm 0.05$) is reached after which higher heterogeneity values has no effect on the PV_{BT} at this optimum injection rate.

4.6. Effect of Presence of Vugs (Large Scale Heterogeneities)

To study the effect of vugs on wormholing in carbonates, the initial porosity profile is modified according to vuggy carbonates characterization results from the Nuclear Magnetic Resonance (NMR) study conducted by Vik et al. (2007). A case with total initial average porosity of 0.3 is designed with random vugs in the medium that accounts for

65% of the total porosity. The vugs are assigned porosity values of 0.9 and the matrix porosity values vary between 0.15 and 0.45. **Fig. 4.12a** shows the initial porosity profile with random distribution of vugs in the 2D domain, and **Fig. 4.12b** presents the wormhole patterns in form of the porosity contour profile after simulation of coreflood injection at an optimum rate.

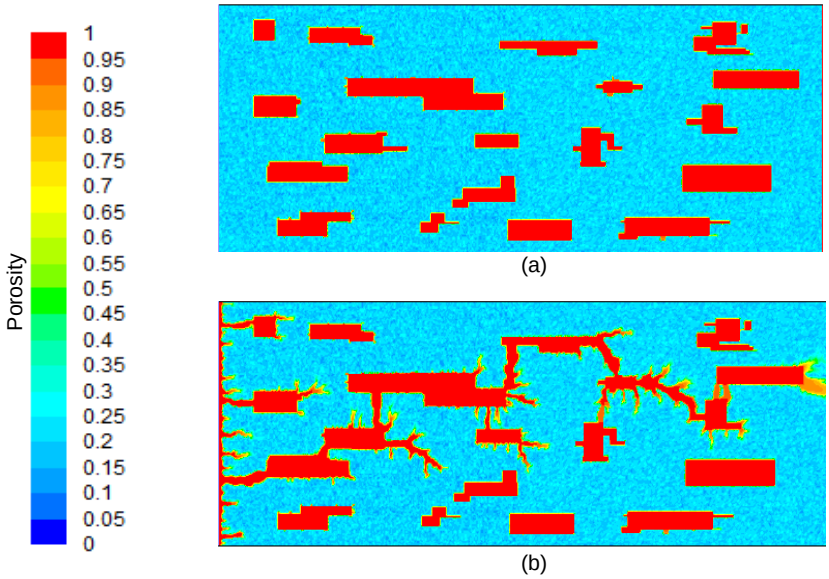

Fig. 4.12–Porosity contour profile showing (a) initial porosity profile of vuggy carbonate core (b) wormhole patterns formed with acid injected at an optimum rate in the vuggy carbonate core.

It is observed from the numerical simulation that acid propagates faster in the vuggy medium than in the uniform heterogeneous porosity medium. This is evident in the plot given in **Fig. 4.13** comparing the acid efficiency curves of both carbonate media with different heterogeneity scales. The diameter of the vugs in the path of the wormhole

determines its diameter. The amount of acid required to breakthrough in the vuggy carbonate is lower than that of a non-vuggy carbonate, which is agreement with experimental results reported by Izgec et al. (2010). Their experimental and numerical work also showed that the wormhole flow path is determined by the local pressure drops created by vugs.

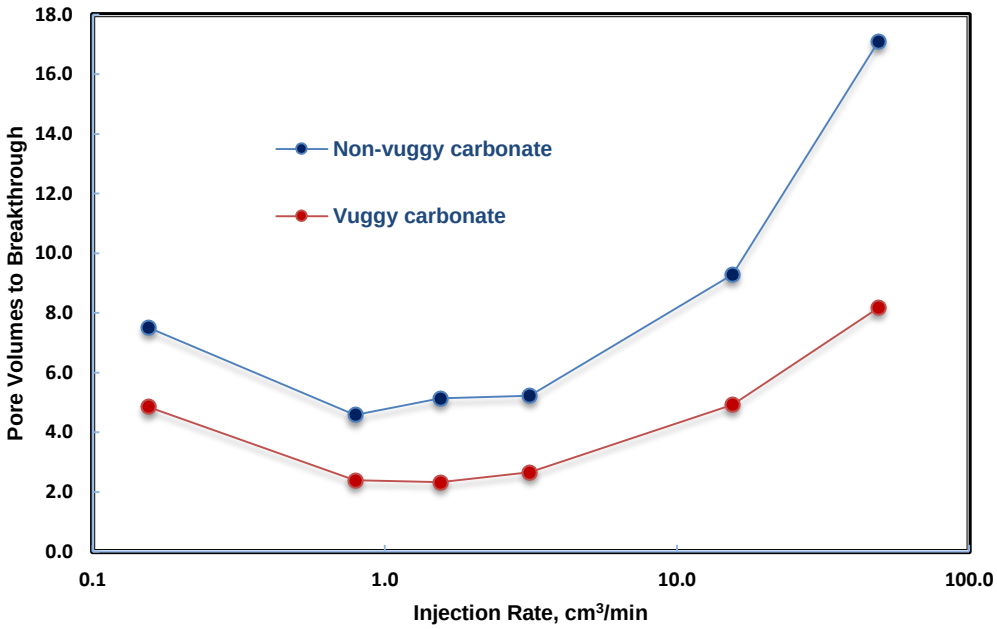

Fig. 4.13–Acid efficiency curves showing the effect of large-scale heterogeneities (vugs) on the pore volumes of acid required to breakthrough.

To conduct further study on the size, amount, and connectivity of the vugs on wormhole propagation, the vuggy porosity profile in Fig. 4.12a is modified as follows:

- Small vugs: The sizes of the vugs are reduced, with the vugs' porosity accounting for 50% of total porosity.
- Larger-sized (big) vugs: The number of vugs are reduced, to make the vugs' porosity account for 50% of total porosity.
- Highly-connected vugs: Some of the vugs are randomly connected to increase connectivity across the medium, keeping the vugs porosity contribution to total porosity at 65% as in the base vuggy porosity profile.

The porosity profiles are given in **Fig. 4.14**. The densely-populated (more) vugs in Fig. 4.14c is the base vuggy porosity profile. Acid coreflood is simulated at an optimum injection velocity of 3.23e-04 m/s for the three additional cases, and the effect of these properties on the amount of acid injected to breakthrough is illustrated by the column chart in **Fig. 4.15**.

The results show that the vuggy rock with the highest connectivity requires the least amount of acid to reach breakthrough, and the homogeneous rock requires the most amount of acid to breakthrough. The size and amount of vugs also influence the amount of acid injected to breakthrough. The bigger the vugs, the lower the amount of acid injected to breakthrough. Also intuitively, the more the amount of vugs present in the medium, the lower the amount of acid injected to breakthrough. The presence of vugs has no effect on the optimum injection rate.

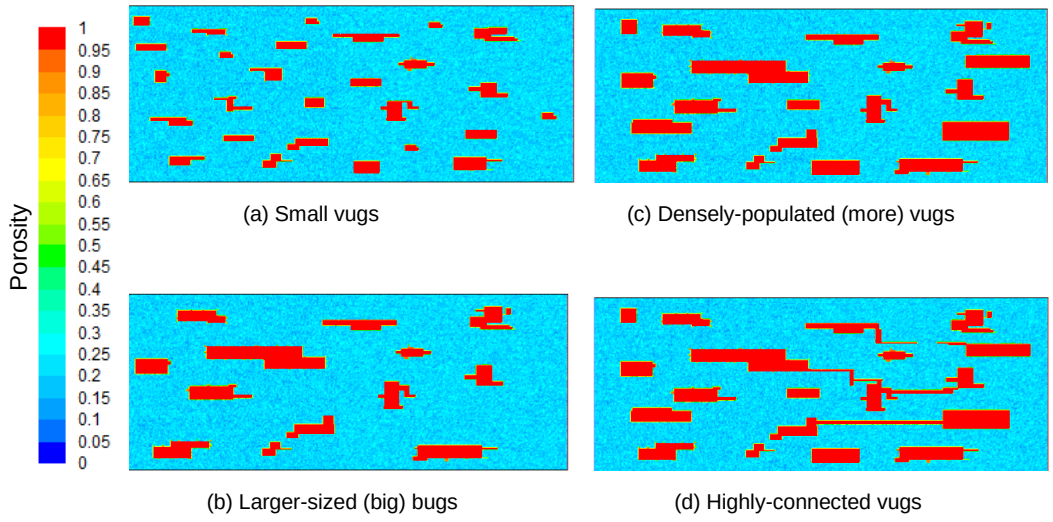

Fig. 4.14–Initial porosity profiles of various vuggy systems to investigate the effect of vugs' size, amount, and connectivity of wormhole propagation.

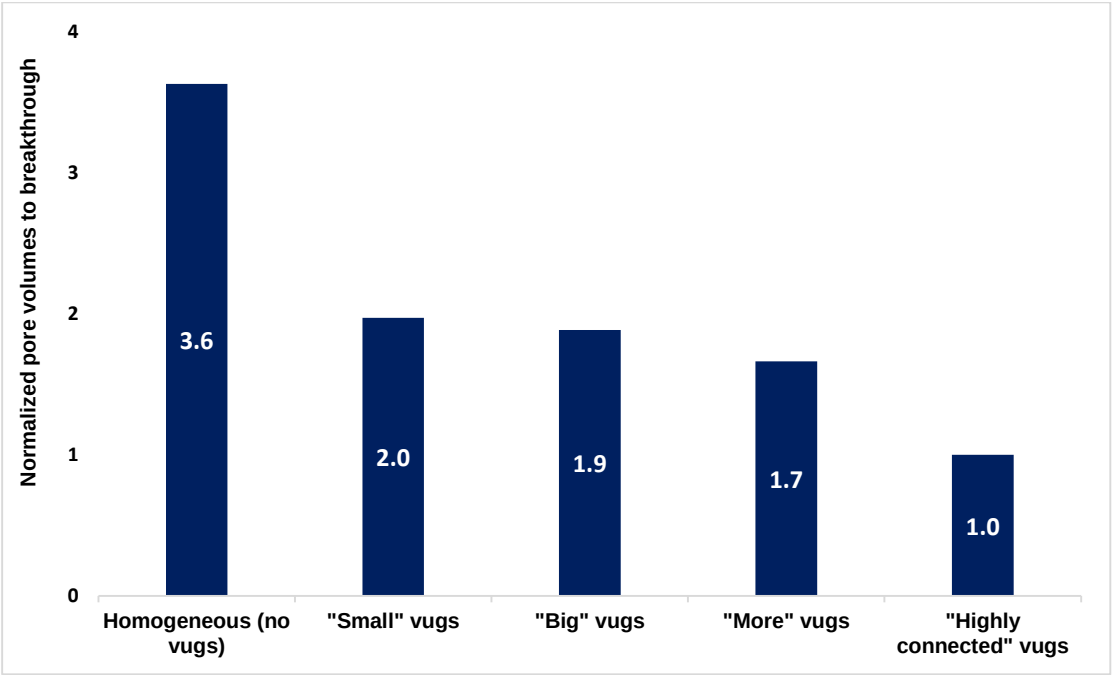

Fig. 4.15–Column chart showing the effect of size, amount, and connectivity of vugs on wormhole propagation.

4.7. Effect of Medium Dimension

Various mesh domains for the 2D model are developed to study the effect of the aspect ratio (core dimensions) on the acid efficiency curve. The aspect ratio is defined as the ratio of the height of the domain to its length. **Fig. 4.16** shows the dimensions of the domains and corresponding aspect ratio values used in this study.

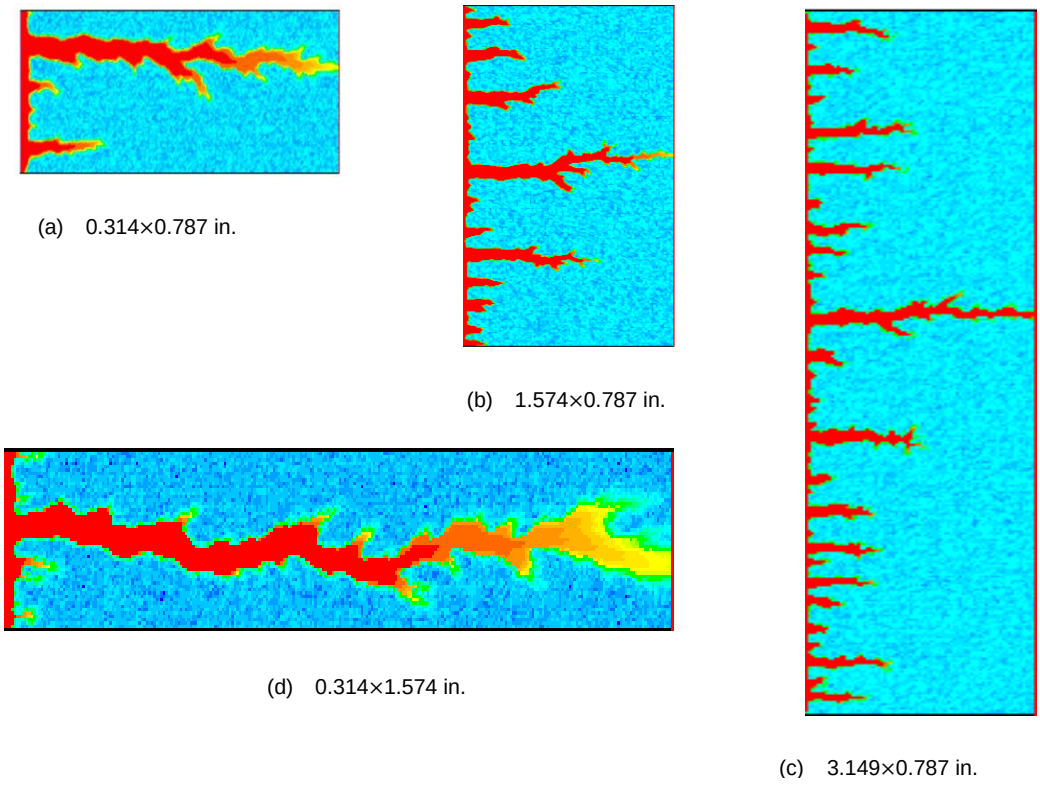

(a) 0.314×0.787 in.

(b) 1.574×0.787 in.

(d) 0.314×1.574 in.

(c) 3.149×0.787 in.

Fig. 4.16–Wormhole patterns for cores with various dimensions with the following aspect ratios (AR): (a) AR = 0.4, (b) AR = 2, (c) AR = 4, (d) AR = 0.2.

The first set of results presented in **Fig. 4.17** show that the value of the optimum injection rate is higher for the long core. The longer the acid propagates in the domain before breakthrough at the outlet, the more the acid is consumed at the walls of the wormhole, so a higher optimum injection rate will be required to transport the acid to the tip of dominant wormhole for longer domains. This trend is in agreement with the conclusion of experimental studies on the effect of core length on the acid efficiency curve by Bazin (2001).

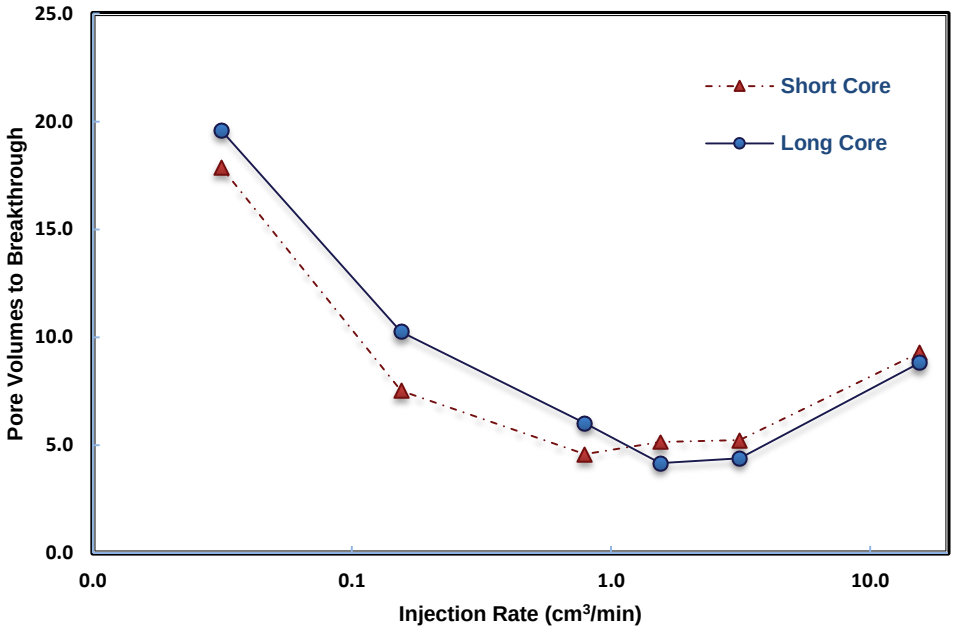

Fig. 4.17–Numerical model results showing the effect of core length on the acid efficiency curve (short core length = 0.787 in. and long core length = 1.574 in.).

Fig. 4.18 presents the results of the effect of the domain height on the acid efficiency curve. The plot shows that PV_{BT} in the wormhole regimes is inversely proportional to the height of the domain. It can be seen from Fig. 4.16 that the number of wormholes initiated at the injection inlet increases with the height of the domain, but only one dominant wormhole reaches the outlet. This means that the fractional amount of solid phase to be dissolved for the acid to reach breakthrough is reduced with an increase in the domain height. At very high injection rates, the PV_{BT} does not depend on the height of the domain because the amount of acid required to reach breakthrough increases proportionally with domain height due to the uniform dissolution of the solid phase. These results are consistent with experimental studies by Furui et al. (2012) on the effect of core diameter on amount of acid injected to breakthrough.

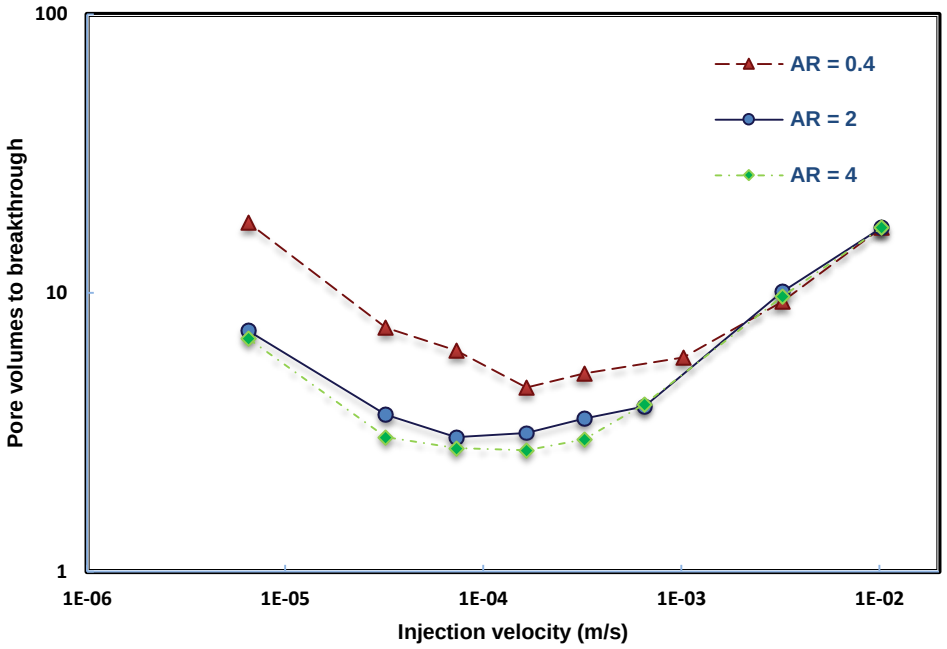

Fig. 4.18–Simulation results showing the effect of the core aspect ratio on the acid efficiency curve [length of core is fixed at 0.787 in.; diameters of the three cases are 0.314 in. (AR = 0.4), 1.574 in. (AR = 2), and 3.149 in. (AR = 4)].

4.8. Effect of Temperature

Experimental studies have been conducted and reported in the literature on the effect of temperature on wormholing during carbonate matrix acidizing. Most of the studies are consistent on the fact that the optimum injection rate and PV_{BT} values are increased at elevated temperatures in the dissolution of limestone by HCl. Wang et al. (1993); Fredd and Fogler (1999); and Bazin (2001) showed that an increase in temperature will cause an increase in optimum injection rate and PV_{BT} values, but Frick et al. (1994) reported that temperature within the range of their experiments had no effect on optimum injection rate while PV_{BT} values decreased with increase in temperature.

To simulate and investigate the effect of temperature on the optimum rate and PV_{BT} values in this work, the effect of temperature on the dissolution rate constant is factored in into the model as following:

$$k_s(T_2) = k_s(T_1)exp\left(\left(\frac{1}{T_1} - \frac{1}{T_2}\right)\frac{\Delta E}{R}\right), \tag{4.1}$$

where k_s is the dissolution rate constants at different temperature values, T_2 and T_1. T_2 = 80°C (353°K), T_1 = 20°C (296°K), k_s = 0.002 m/s. ΔE is the activation energy and R is the gas constant. ΔE/R = 7550°K (Schechter 1992).

The acid diffusivity relation is given by the relation (Kalia and Glasbergen 2009)

$$\frac{D_{m_2}}{D_{m_1}} = \frac{\mu_1}{\mu_2}\frac{T_2}{T_1}, \tag{4.2}$$

where D_{m1} and D_{m2} are acid diffusivity values at different temperatures T_1 and T_2, respectively, and μ_1 and μ_2 are the acid viscosity values at T_1 and T_2, respectively.

The numerical simulation results from the two-scale model given in form of the acid efficiency curves **Fig 4.19** show that the optimum injection rate is considerably higher at 80°C than at 23°C, and the PV_{BT} values are higher at higher temperatures for rates at and below the optimum injection rate as expected.

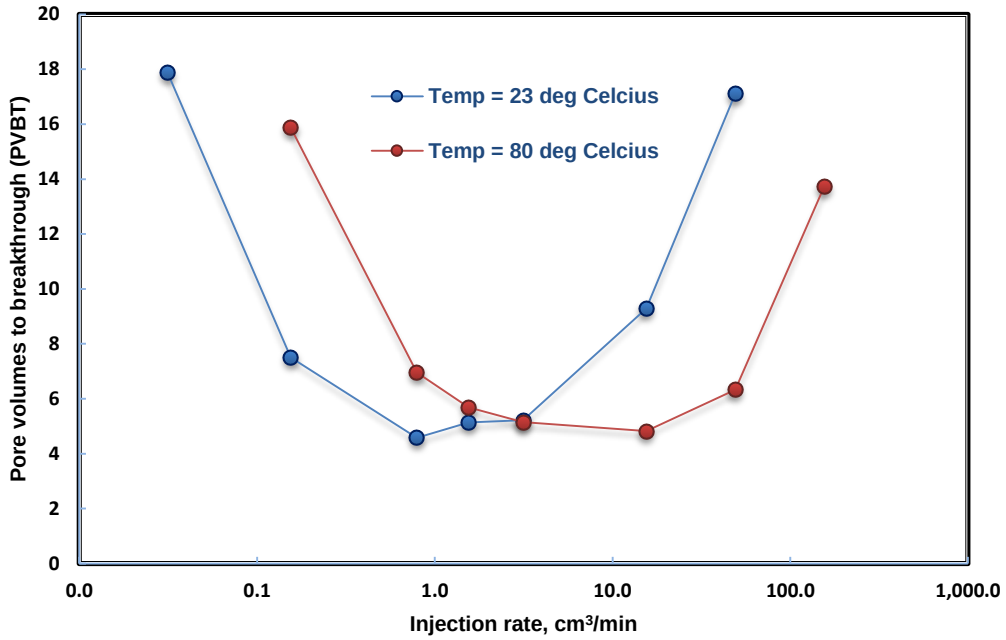

Fig. 4.19–Effect of temperature on optimum injection rate and pore volumes of acid injected to breakthrough.

4.9. Effect of Acid Concentration

The effect of acid concentration, in form of reaction rate constant, on the optimum injection rate and PV_{BT} values are examined. Three cases with different reaction rate constants are simulated, and the resulting acid efficiency curves are presented in **Fig. 4.20**. To reach the dominant wormhole regime, the faster reacting acid will have to be injected at a higher rate than a slower reacting acid for most of the acid to be transported to the tip of the wormholes and not be totally consumed along the walls of the wormholes.

Previous experimental studies have shown that wormholes created by highly reactive acid are thinner and more branched than those created by slow-reacting acid. This leads to lower PV_{BT} values and higher optimum injection rates at the wormhole regimes for acids with higher reaction rate constants. This trend in Fig 4.20 is similar to that

observed in the experimental studies by Bazin (2001) and Furui et al. (2012) on the effect of acid concentration (which determines acid reactivity) on the acid efficiency curve.

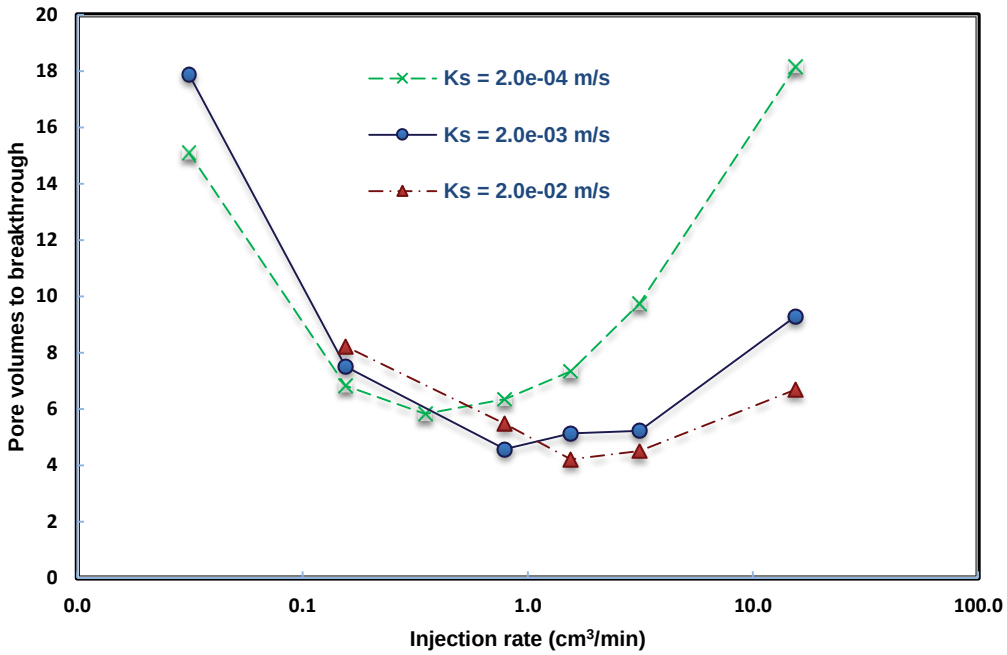

Fig. 4.20–Numerical model results showing the effect of reaction rate constant on the acid efficiency curve.

4.10. Section Conclusions

The following conclusions are drawn from the simulation results of the modified model developed in this study:

1. The Navier-Stokes momentum formulation can be used to effectively describe fluid flow in the two-scale model, and the model in this work captures all the dissolution patterns that occur during carbonate matrix acidizing. The

computational time required to achieve breakthrough in the ramified and uniform dissolution regime with the Navier-Stokes formulation is lower than that required using the Darcy's law based formulation.

2. Sensitivity tests conducted on the model for various factors that affect wormhole propagation during carbonate acidizing provided results consistent with experimental observations and previous two-scale models with fluid flow described by Darcy's law.
3. The simulation results from this study show that the geometry of flow affects the dissolution process and determines the optimum injection rate with the amount of acid required to achieve breakthrough. Thus, the linear flow modeled in laboratory experiments is not representative of radial flow, which occur in field conditions.
4. The effects of initial average porosity and formation heterogeneity on the pore volumes of acid injected to breakthrough in a coreflood experiment were presented from the simulation output. The model also showed how the core dimensions influence the optimum injection rate and pore volumes of acid injected to breakthrough in coreflood experiments. This should be accounted for in the translation of optimum injection rates obtained from coreflood experiments to field applications.
5. Reaction rate kinetics influence the wormholing process, as was demonstrated by the model. The optimum injection rate increases as the reactivity of the acid, in form on the reaction rate constant, increases and the amount of acid required to achieve breakthrough is reduced.

5 APPLICATION OF THE TWO-SCALE MODEL TO ALTERNATIVE ACIDIZING FLUIDS

5.1. Introduction

The acidizing fluid that has been studied so far with the two-scale carbonate acidizing model is HCl. Ratnakar et al. (2013) modeled wormhole formation in carbonates by situ cross-linked acid and Maheshwari et al. (2014) studied the reactive-dissolution modeling of carbonate acidizing with gelled and emulsified acids with the two-scale approach. For these two studies, the base acid in the retarded acid system was HCl, with first-order irreversible reaction assumed in modeling the reaction kinetics.

In this section, we examine the effect of order of reaction on the model output for wormhole propagation, and then extend the two-scale model for acetic acid, which has a more complex reaction chemistry than acidizing fluid systems with HCl as the base acid. We also examine application of the two-scale model to chelating agents with simplified reaction kinetics.

5.2. Order of Reaction

For the cases presented so far in this study, linear first-order kinetics is assumed, and the output has been shown in the previous section to agree qualitatively with experimental results. Here, a nonlinear reaction kinetics model is used in which:

$$R(C) = k_s C_s^n, \tag{5.1}$$

where n is the order of reaction.

The simulation results showing the effect of the order of reaction on the acid efficiency curve are presented in **Fig. 5.1**. It can be seen that the higher the order of reaction, the lower the optimum injection rate and amount of acid required to achieve breakthrough. The fractional order of reaction in the model reduces the concentration of acid available for dissolution of calcite (to increase porosity) so the time taken to breakthrough at the outlet is longer and the amount of acid injected more than it would be for a first order kinetics equation. As noted by Maheshwari et al. (2012), there is no agreement in literature about the magnitude of reaction rate constant and order of reaction for the dissolution of limestone, but the simulation results show that the order of reaction significantly influences the PV_{BT}.

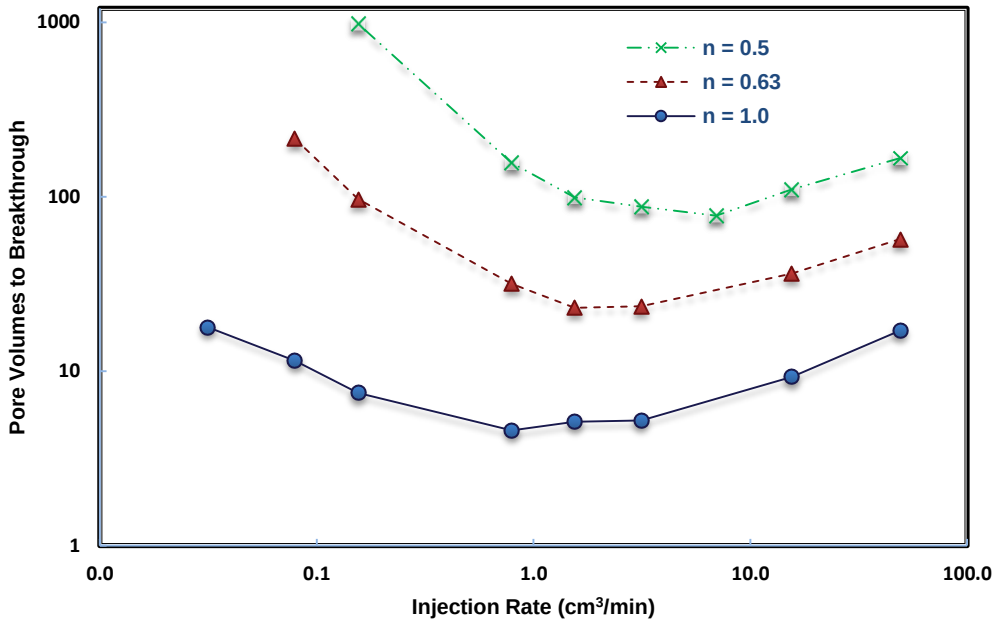

Fig. 5.1–Numerical model results showing the effect of order of reaction on the acid efficiency curve.

5.3. Alternative Acidizing Fluids

The use of HCl will not be feasible for a successful carbonate matrix acidizing treatment in some situations where lower injection rates are required, or when acidizing fluids with lower reactivity is needed to avoid corrosion on the well completion materials at high temperature conditions. Alternative acidizing fluids such as organic acids and chelating agents have been used with success instead of HCl but no proper carbonate acidizing model has been developed for the use of these acid systems. In the section, the two-scale model is modified and applied for acetic acid (organic acid), ethylenediaminetetraacetic acid (EDTA) and diethylenetriaminepentaacetic acid (DTPA).

5.3.1. Acetic Acid

The simple linear first-order reaction kinetics model cannot be applied for organic acids, because weak acids such as organic acids do not dissociate completely in aqueous solution, therefore the dissociation equilibrium has to be considered in their reaction kinetics with carbonates.

The dissociation of an acid in aqueous solution can be represented by the reaction in Eq. (5.2) below:

$$\mathrm{HA} \rightleftharpoons \mathrm{H^+} + \mathrm{A^-}. \tag{5.2}$$

The dissociation (equilibrium) constant, K_d, is expressed by

$$K_d = \frac{a_{\mathrm{H^+}} a_{\mathrm{A^-}}}{a_{\mathrm{HA}}}, \tag{5.3}$$

where $a_{\mathrm{H^+}}$ and $a_{\mathrm{A^-}}$ denote the activities of the H^+ and A^- ions respectively.

The kinetics for acetic acid-limestone reaction is given by (Schechter 1992)

$$R(C_{HAc}) = k_s K_d^{n/2} C_{HAc}^{n/2}. \quad (5.4)$$

The dissociation constant, a function of temperature (T in °K), can be obtained from Eq. (5.5):

$$-log_{10} K_d = \frac{A_1}{T} - A_2 + A_3 T. \quad (5.5)$$

The values of the constants A_1, A_2, and A_3 are given as 1170.48, 3.1649, and 0.013399 respectively (Schechter 1992).

The first order linear kinetics equation in the two-scale model is replaced by Eq. (5.4) for acetic acid-limestone reaction. The model is updated with values of dissolution rate constant, acid diffusivity, density, viscosity for acetic acid at pH of 2.5 and 4.6. The PV_{BT} values from the 2D simulation results of this modified model for acetic acid (pH 2.5 and 4.6) is normalized with previous HCl PV_{BT} values and the acid efficiency curves plotted alongside experimental results from Fredd and Fogler (1999).

The model output matches well with the experimental results (**Fig. 5.2**) except at the extreme values of injection rates (the simulation results are represented by the solid lines and experimental data by marker points). This slight mismatch could be due to how the PV_{BT} values are obtained from the model (when pressure drop across domain drops to $1/100^{th}$ of its initial value) which will give PV_{BT} values lower than experimentally obtained ones because of the additional time in experiment which acid physically breaks through at the outlet of the core.

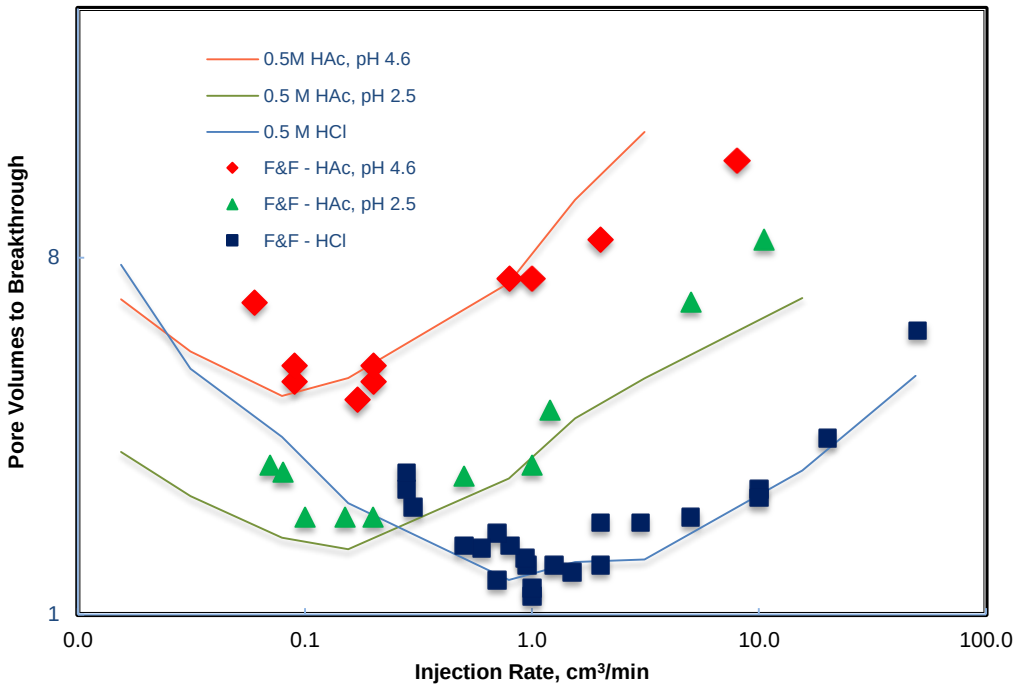

Fig. 5.2–Normalized model results comparing the acid efficiency curves of HCl and acetic acid with experimental work from Fredd and Fogler (1999).

5.3.2. Chelating Agents

The multi-step chemistry at the solid-fluid interface that occurs during the chelating process of the dissolution of limestone by chelates is complicated and not representable by any available kinetics equation in the literature. In this section, the linear first order reaction kinetics equation is used to simulate calcite acidizing with EDTA and DTPA. The fluid properties in the model are changed to those of EDTA and DTPA (values obtained from Fredd and Fogler 1999) as given in **Table 5.1**.

Acidizing fluid	Acid diffusivity (m^2/s)	Reaction rate constant (m/s)	Initial acid concentration (inlet)
0.25 M EDTA (pH 4)	6e-10	1.4e-06	0.0848
0.25 M DTPA (pH 4.3)	4e-10	4.8e-07	0.0655

Table 5.1–Fluid properties of chelates updated in model.

Fig. 5.3 shows that acid efficiency curves from the numerical simulation of EDTA and DTPA as acidizing fluids does not match with experimental results from Fredd and Fogler (1998) as well as that of HCl. This trend is expected because the first order kinetics equation used is more representative of the reaction of HCl-calcite than that of chelates-calcite. A more complex multi-step chemistry is involved in the dissolution by chelates.

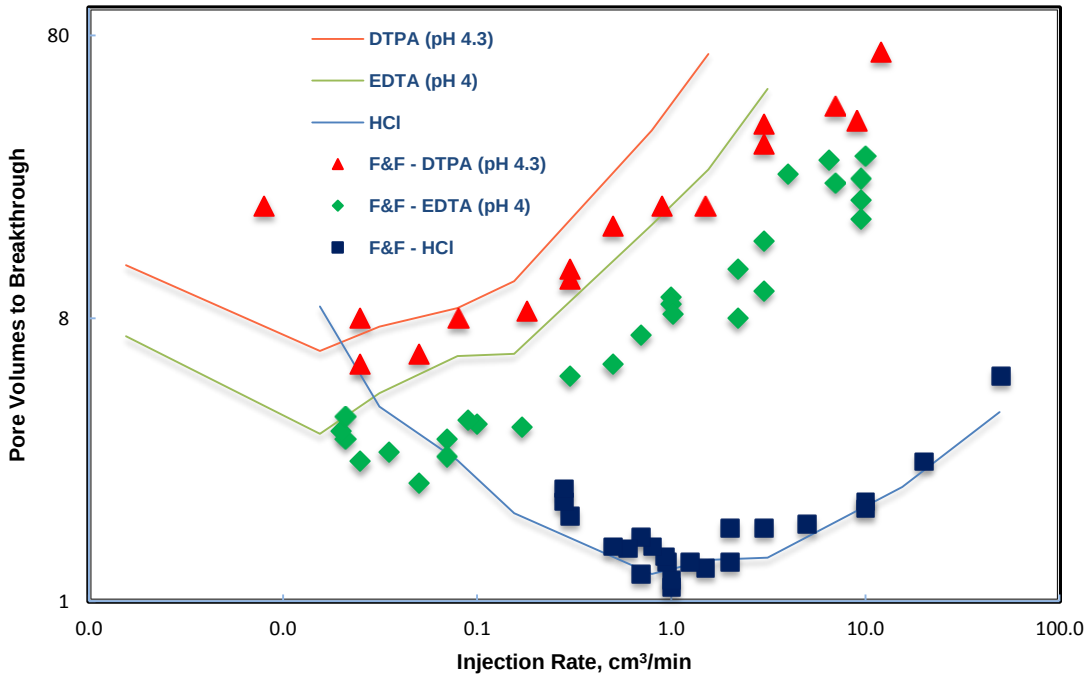

Fig. 5.3–Normalized model results comparing the acid efficiency curves of HCl and chelating agents (EDTA and DTPA) with experimental results from Fredd and Fogler (1998).

5.4. Section Conclusions

In this section, the reaction kinetics of the model was modified to extend it for alternative acidizing fluids. Here are the conclusions from the results:

1. Simulation results showed that higher PV_{BT} values are obtained when lower fractional values of the order of reaction are used in the reaction kinetics equation of the model. This is because the fractional order of reaction in the model reduces the concentration of acid available for dissolution of calcite (to increase porosity), therefore more acid will be required to be injected to achieve breakthrough than would be for a first order kinetics equation.
2. To apply the two-scale model for acetic acid, the use of the Schechter (1992) reaction kinetics equation of organic acids and calcite produces normalized simulation output that are in agreement with experimental results.
3. The complex multi-step chemistry in the dissolution of calcite by chelating agents is not easily modeled in the two-scale approach, and the normalized simulation results from the application of first order kinetics in the model does not match perfectly with experimental results.

6 ACIDIZING FLUID AND ADDITIVES SELECTION FOR CARBONATE MATRIX ACIDIZING

6.1. Acid Screening Criteria

The use of HCl as the acidizing fluid is the first option considered in carbonates matrix acid treatment because it has a high dissolving power, it is inexpensive compared to other acidizing fluids, and is readily available. The acid selection chart in **Fig. 6.1** is designed to check the feasibility and efficiency of using HCl before considering other alternatives such as organic acids, chelates, or other retarded acid systems.

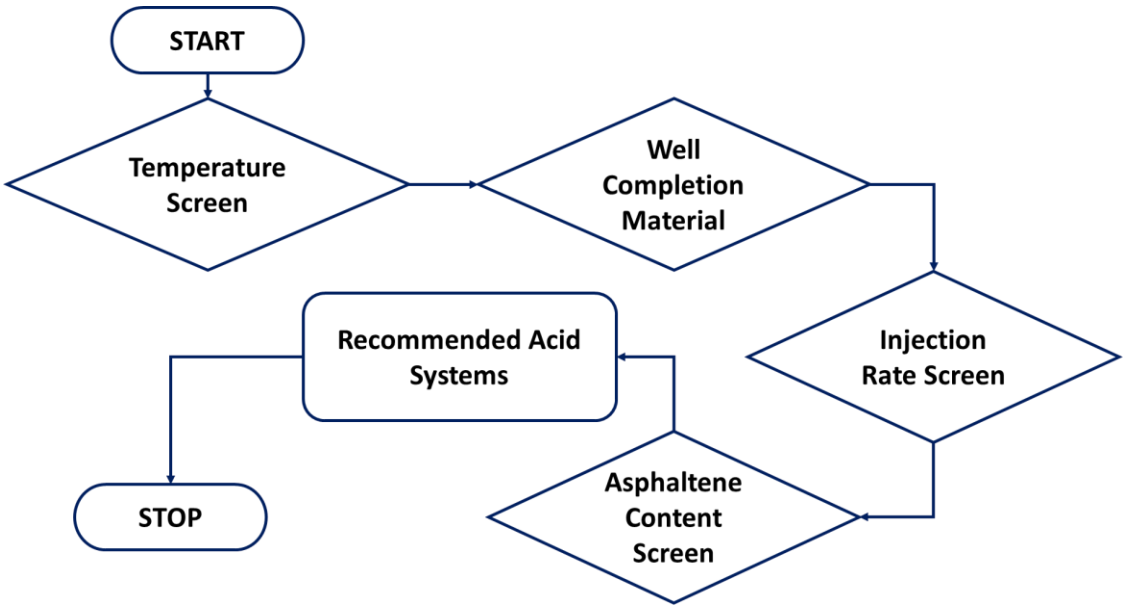

Fig. 6.1–Acid selection chart showing screening factors for acidizing fluids.

The factors listed below, also shown in the Fig. 6.1 are the screening criteria to determine which acidizing fluid(s) can be used in the treatment:

- Formation Temperature
- Well Completion Material
- Injection Rate (from optimum and maximum-allowable injection rates)
- Asphaltene Content (in crude oil)

The listed factors are discussed with their application in screening for the selection of the acidizing fluid.

6.1.1. Formation Temperature

The temperature of the formation is a decisive factor in designing a matrix acid treatment. The rock dissolution rate in the presence of acid depends on the temperature at which the reaction takes place for both limestone and dolomite (Lund et al. 1973). Rocks dissolve at a faster rate at elevated temperatures, and this determines whether the acid treatment will lead to the formation of wormholes for a successful treatment or uniform/face dissolution for an unsuccessful one.

The reservoir temperature also plays a role in the selection of the acidizing fluid based on the tubular type used in the completion of the well. The selection of additives and intensifiers to accompany the acidizing fluid are also affected by the formation temperature.

The temperature screen can be split into three limits (based on a fluid selection chart by Thomas and Morgenthaler 2000) to determine whether the following

concentrations of HCl (except for temperatures above 350°F) can be used without the need to consider other acid systems:

- If the bottomhole temperature is below 300°F, then 28 and 15 wt% HCl can be used
- If the bottomhole temperature is between 300 and 350°F, then 15 or 10 wt% HCl, or a mixture of HCl and acetic acid can be used
- If the bottomhole temperature is above 350°F, then an organic mixture of 13% acetic acid + 9% formic acid (same dissolving power as 15 wt% HCl) is recommended, according to Van Domelen and Jenning (1995).

6.1.2. Well Completion Material

The completion material used in the well tubing is also an important factor in deciding the type of acid system that can be used in the treatment. The common materials used in well tubulars are low carbon steel, chromes, and nickel alloys.

6.1.2.1. Carbon Steel

Steel is a mixture of iron and carbon by definition, and carbon steel is steel with no alloy metals added. It becomes alloy steel is when other elements such as chromium, molybdenum, nickel, vanadium are added. Low carbon steel contains between 0.05 - 0.3% carbon, and mild carbon steel contains between 0.3 - 0.6% carbon. The most commonly used carbon steel material in production well tubulars is N80. It is used in non-corrosive environments where moderate strength is required.

6.1.2.2. Chromes

Chrome is steel alloy employed in high temperature and high pressure conditions. Chromium is added to steel to improve corrosion resistance, strength, and response to extremely high temperature. At 3-10% chromium, steel resists corrosion; at 10.5-20%, the steel is fully stainless. Chromes are suitable for use in oilfield environments containing chlorides, carbon dioxide, and traces of hydrogen sulfate. Examples of chrome alloys include 9Cr, 13Cr, 22Cr, and 25Cr.

6.1.2.3. Nickel Alloys

Nickel alloys are alloys based on nickel as the main element, with other metals or materials added to improve the properties of the alloys for specific functions. Nickel alloys are extensively used due to their high corrosion resistance, even at very high strength levels, and also for their high thermal expansion properties. Examples of nickel alloys used in well completion in the oilfield include 625, 718, 825, 925, and K500.

6.1.2.4. Corrosion Rates

When in contact with HCl and other acidizing fluids, during the acid treatment process, these alloys used in the well tubulars corrode and the rate of corrosion is dependent on the temperature. In high temperature acidizing, a corrosion rate less than 2,000 mpy (50.8 mm/yr) is acceptable (Hinshaw et al. 2011). **Table 6.1** shows the acceptable corrosion rates with respect to temperature according to Smith et al. (1978).

Temperature (°F)	Corrosion Rate (lb/ft^2/test period)
< 200	0.02
- 250	0.05
251 - 275	0.075
> 276	0.09

Table 6.1–Acceptable corrosion rate (reprinted with permission from Smith et al. 1978. Further reproduction prohibited without permission.)

The summary of tests on N80, 13Cr, 22Cr with different concentrations of HCl, at various temperatures in the presence of corrosion inhibitors plus intensifiers is presented in Appendix A.

According to previous experimental studies on the limitations of the use of HCl with chrome alloys, 28 wt% HCl should not be used with chrome alloys, and HCl (any concentration) should not be used with 22Cr and 25Cr chrome alloys. This information, with the corrosion results test summary from Appendix A, is summarized in **Table 6.2** as part of the selection screen in using HCl for acidizing in the presence of carbon steel and chrome alloy tubular in the advisory program.

Acid	N80	13Cr	22Cr	25Cr
28% HCl	YES (<290°F)	NO	NO	NO
15% HCl	YES (<400°F)	YES (<350ºF)	NO	NO
10% HCl	YES	YES	NO	NO

Table 6.2–Chrome alloy tubulars and N80 temperature limits with HCl.

For Nickel-Based Alloys, Iconel 718 shows as much corrosion resistance to HCl as other alloys of chromium (13Cr-S110, 13CR-M110, 13Cr95, 13Cr95 and 22Cr) (Seth et al. 2011).

6.1.3. Injection Rate

The injection rate determines how well wormholes form in the treatment process. For an optimum treatment, the injection rate must be at, or slightly above, the optimum rate of the fluid-mineral-temperature system. The injection rate must also be below the maximum allowable injection rate of the formation due to fracture constraint. The maximum allowable injection rate is calculated from the fracture pressure at bottomhole pressure (Eq. 2.12 and 2.13).

If the optimum injection rate is unknown, the maximum allowable injection rate is used as the optimum injection rate. It is better to inject at a rate higher than the optimum injection rate than below. The maximum allowable injection rate is calculated from the fracture pressure and the optimum injection rate can be estimated using the Transition pore theory/Damköhler number approach (Eq. 2.3) for lower temperature formations.

6.1.4. Asphaltene Content

The presence of asphaltene in crude oil could be detrimental during an acidizing process. Asphaltenes are the heaviest component of a crude oil. They are large polyaromatic polar compounds often containing nitrogen, oxygen, and sulfur in the structure. They also may contain heavy metals such as nickel, vanadium, and others (Hashmi and Firoozabadi 2011). In addition to these elements, asphaltenes have been shown to contain a significant amount of acid/base functional groups. An asphaltene has

been defined as the component of the crude oil that is soluble in aromatic solvents (benzene, toluene, xylene) but insoluble in short-chained aliphatics (n-pentane, n-heptane) (Chang and Fogler 1994).

The interaction between the acidizing fluid and crude oil can lead to two major damage mechanisms, which then results in the failure of the matrix acidizing treatment of the oil well. These mechanisms are the precipitation of acid induced asphaltene sludge and formation of rigid film emulsions.

Asphaltene precipitation is especially prolific when a strong acid mixes with certain crude oils. As the concentration of acid increases, the potential for sludging significantly increases. The presence of iron, specifically ferric dissolved in acid, has been proven to exponentially increase asphaltene precipitation (Lalchan et al. 2013).

According to work done by Houchin et al. (1990) and Strassner (1968), acid induced sludge occurs on crudes with API gravities ≥ 27 and asphaltene contents of $\leq 3\%$ by weight. Rigid film emulsions form whenever asphaltene containing crude comes in contact with an aqueous fluid of $pH \leq 6$. Crude oil with API gravities ≤ 22 and asphaltene contents of $\geq 4\%$ by weight typically form rigid emulsions and subsequently do not sludge.

In the selection of an acidizing fluid, if the asphaltene content of the crude show that the use of the high concentration of HCl could lead to sludging or emulsions then other acidizing fluids are suggested to be used in the treatment.

6.2. Acidizing Fluids

Acidizing fluids systems used in matrix acidizing can be classified as mineral acids, organic acids, powdered organic acids, hybrid acids, retarded acids, and chelating agents (Schechter 1992).

6.2.1. Mineral Acids

The commonly used acid in carbonate acidizing is HCl. 28 wt% HCl is used to treat deep wellbore damage, but 15 wt% HCl is usually used in most carbonate acidizing treatment. The main disadvantage of HCl is its high corrosivity on well completion materials. Other limitations include rapid acid spending at low injection rates, which leads to face dissolution, formation of asphaltic sludge, and rigid film emulsions in crude oil containing asphaltenes.

6.2.2. Organic Acids

Organic acids, such as formic and acetic acid, are used to offer slower reacting, and deeper stimulating acids. It also offers lower corrosivity at high temperatures. Acetic acid is a commonly used organic acid in carbonate matrix acidizing, and it can used in mixtures with HCl for stimulation. Acetic acid is more expensive than HCl or formic acid, limiting its use for initial application. Formic acid is less expensive than acetic acid, but this advantage is offset by the greater difficulty of inhibiting corrosion with formic acid. The reaction of organic acids with limestone not irreversible, as in the case with HCl, and the reaction products can precipitate at certain conditions. This may form on the rock surface and act as a barrier which hinders further dissolution of the rock by the acid (Li et al. 2008).

6.2.3. Powdered Acids

Powdered acids are white crystalline powders readily soluble in water for use at the injection site (Schechter 1992). Sulfamic and chloroacetic acids are common examples of powdered acids used in carbonate acidizing. These acids have limited applications in well stimulation, most of which is associated with their portability to remote locations in powdered forms. Both acids are more expensive than HCl. Chloroacetic acid is the organochloride compound with the formula $ClCH_2CO_2H$ and it is industrially known as monochloroacetic acid (MCA). Sulfamic acid is a molecular compound with the formula $HOSO_2NH_2$. Sulfamic acid decomposes to ammonium acid sulfate at about 80°C (Clapp 1943), and is not recommended for applications with formation temperatures greater than 70°C.

6.2.4. Mixed Acids

Mixed acids can be used instead of standalone acids such as HCl to obtain the same dissolving power at a lower corrosivity. Examples of mixed acids include acetic-hydrochloric, formic-hydrochloric, or acetic-formic acids. They are mostly used in high temperature conditions where the corrosion inhibition cost is of high significant compared to the overall cost of treatment (Schechter 1992).

6.2.5. Retarded Acids

There are various ways to slow (or retard) the acid reaction rate. The diffusion of acid to the rock surface can be slowed by increasing the viscosity (in form of gelling), the acid can be emulsified with oil creating an acid-oil emulsion, or the coating of the rock surface with an adsorbed layer of inert molecules to decrease the rate at which acid reaches

the rock surface. Examples of retarded acid systems include foamed, emulsified, and gelled acids.

6.2.6. Chelating Agents

Chelating agents can be used in acidizing treatments in place of HCl in situations where the use of HCl is limited as previously explained. Examples of chelating agents are as follows: Ethylenediaminetetraacetic acid (EDTA), hydroxyethyl ethylenediamine triacetic acid (HEDTA), cyclohexylene-aminotetraacetic acid (CDTA), diethylenetriaminepentaacetic acid (DTPA), and GLDA (L-glutamic acid-N,N-diacetic acid), and they have been demonstrated in previous works for stimulating carbonate formations. Chelates complex with calcite and form water-soluble products.

The following models have been developed to study the mechanism of calcite dissolution by chelating agents: the Li et al. (2008) EDTA model, the Frenier et al. (2001) model, and the Wu and Grant (2002) model.

Mahmoud and Nasr-El-Din (2012) developed an analytical model that describes the flow of HEDTA and EDTA chelating agents and the propagation inside carbonate formations. They concluded that the model can be used to determine the best stimulation fluid based on the temperature and fracture pressure of the target zones.

6.3. Additives

No acidizing fluid is pumped downhole without additives. These additives can be used to aid in the penetration of the fluid or to perform other functions in the acidizing treatment process. Additives can be used to prevent corrosion, prevent sludging and emulsions, prevent iron precipitation, improve wellbore cleanup, improve coverage of the

zone to be acidized, and also prevent precipitation of reaction products during and after stimulation.

For any acidizing fluid to be pumped from through the tubing and into the formation, corrosion inhibitors must be added to prevent the corrosion of the completion material by the acidizing fluid. Additives such as corrosion inhibitor intensifiers, surfactants, solvents, iron control agents, non-emulsifiers and others could be used alongside the corrosion inhibitor (Frenier and Hill 2002). These additives have an effect on the reaction dissolution rate during carbonate acidizing, and thus the efficiency of the wormhole propagation if not properly accounted for in the design process.

6.3.1. Mandatory Additives

6.3.1.1. Corrosion Inhibitors

A corrosion inhibitor is the additive used with the acidizing fluid to limit the attack of acid corrosion on drill pipes, tubing, or any other metal that comes in contact with the acid during the acidizing procedure. They are the most important additives. The corrosion inhibitor cost is often a large percentage of the total treatment cost, especially at high temperature conditions or in long acid-pipe contact situations (Schechter 1992).

The additives present in the acid system can modify the effectiveness of the corrosion inhibitor. Materials such as mutual solvents or surfactants often alter the effectiveness of corrosion inhibitor by preventing or aiding in the inhibitor adsorption. The selection of inhibitor type and concentration should be made with consideration to the following conditions:

- Type and concentration of acid

- Completion materials exposed to acid
- Maximum pipe temperature
- Duration of acid-pipe contact

Corrosion inhibitors affect the dissolution rate of the acid system on the rock. According to experimental results reported by Taylor et al. (2004), a 2 vol% corrosion inhibitor decreased the calcite dissolution rate by approximately 9%. This is an important factor to consider in designing an acid system.

6.3.1.2. Corrosion Inhibitor Intensifiers

Intensifiers are used with acid corrosion inhibitors to enhance the efficiency of the inhibitor at high temperatures. They are used to extend the safe contact time available during the treatment process, allow the corrosion inhibitor to function in very strong acids, and also to allow the inhibitor to be used in the presence of chrome alloys (Brezinski 1999). Formic acid is one of the more commonly used intensifiers. Other examples include Copper salts, potassium iodide, and acid soluble mercury metal salt.

6.3.1.3. Iron Control Additives

Ferric ions re-precipitate as gelatinous, damaging, ferric hydroxide whenever the pH of spent acid solution rises above 2 during an acid treatment (Ali and Hinkel 2000). The precipitation of gelatinous ferric hydroxide can be prevented by adding certain complexing or sequestering agents to the acid. Several organic acids (citric, lactic, acetic, and gluconic) and their derivatives ethylenediaminetetraacetic acid (EDTA) and nitrilotriacetic acid (NTA) are considered useful sequestering agents.

6.3.2. Conditional Additives

6.3.2.1. Surfactants

Surfactants are used in acidizing to perform various tasks such as the following: Reduce surface and/or interfacial tension, break undesirable emulsions, alter wettability, disperse additives, and prevent sludge formation in the presence of asphaltene. Careful surfactant selection is essential because an improper surfactant can result in in unwanted outcome that could hinder the success of the acid treatment.

6.3.2.2. Mutual Solvents

Mutual solvents are chemicals that are mutually soluble in both water and hydrocarbon. The most efficient and preferred mutual solvents are glycol ethers (containing at least a butyl or higher molecular weight group), which is a reaction product of alcohols and ethylene oxide.

Experimental results showed that 10 vol% mutual solvent increased the acid dissolution rate by 9% for calcite and by up to 29% for dolomite (Taylor et al. 2004).

6.3.2.3. Diverting Agents

To achieve maximum stimulation of the formation from a matrix acidizing treatment, it is essential to treat the entire production interval. When several sands are open to the wellbore or the section to be treated is massive, it is necessary to divide the treatment into stages. Diverting agents are designed to act as bridge at the formation pores during carbonate matrix acidizing.

Experimental results reported by Taylor et al. (2004) showed that 1.5 vol% cationic acrylamide polymer decreased the carbonate dissolution rates significantly. At 1000 rpm, the limestone dissolution rate with 0.1 N HCl reduced by 11.4% when 1.5 vol% polymer is added. It is concluded that the addition of the polymer to the acidizing fluid changed the acid-rock reaction from mass transfer limited to surface reaction for carbonates. They attributed this effect to polymer adsorption on the rock surface.

6.3.2.4. Calcium Sulfate Scale Inhibitors (*with Calcium Chloride*)

When calcium sulfate in the form of anhydrite ($CaSO_4$) or gypsum ($CaSO_4.2H_2O$) is present in the formation, the problem of re-precipitation may arise because this sulfate is less soluble in spent acid than in live acid. This re-precipitation of calcium sulfate during carbonate acidizing, on spending, can be minimized by the addition of calcium chloride to the calcium scale inhibitors used in the acidizing fluid system (Delorey et al. 1996).

6.3.2.5. Anti-Sludge Agents

If asphaltene is present in the crude oil, anti-sludge agents are added to the acidizing fluid to prevent the precipitation of acid-induced asphaltene sludge or formation of rigid film emulsions.

6.3.2.6. Biocides

Bacteria are present naturally in various parts of production operations. Examples of such bacteria are SRB (Sulfate-Reducing Bacteria) which convert iron from ferrous to ferric form and precipitate ferric hydroxide during the acidizing treatment. Biocides can also be added to the acidizing fluid to reduce the damage that can be caused to the formation by bacteria.

6.3.2.7. Hydrogen Sulfide Scavengers

Hydrogen sulfide (H_2S) scavengers are used to mitigate the effect of H_2S which can be produced from the reaction between the acid and iron sulfide scale existing in the formation. Hydrogen sulfide produced with the spent acid is very risky for health and environment in addition to the risk of creating stress corrosion cracking with materials in the well.

6.4. Additives Selection Chart

An additives selection chart classifying mandatory and conditional additives with the conditions in which they are to be used is presented in **Fig. 6.2**. All additives added to the acidizing fluid to be pumped downhole should be tested in the laboratory with well and reservoir conditions simulated as much as possible. The additives selection chart is only to provide the engineer an idea of the additives to be considered in general cases.

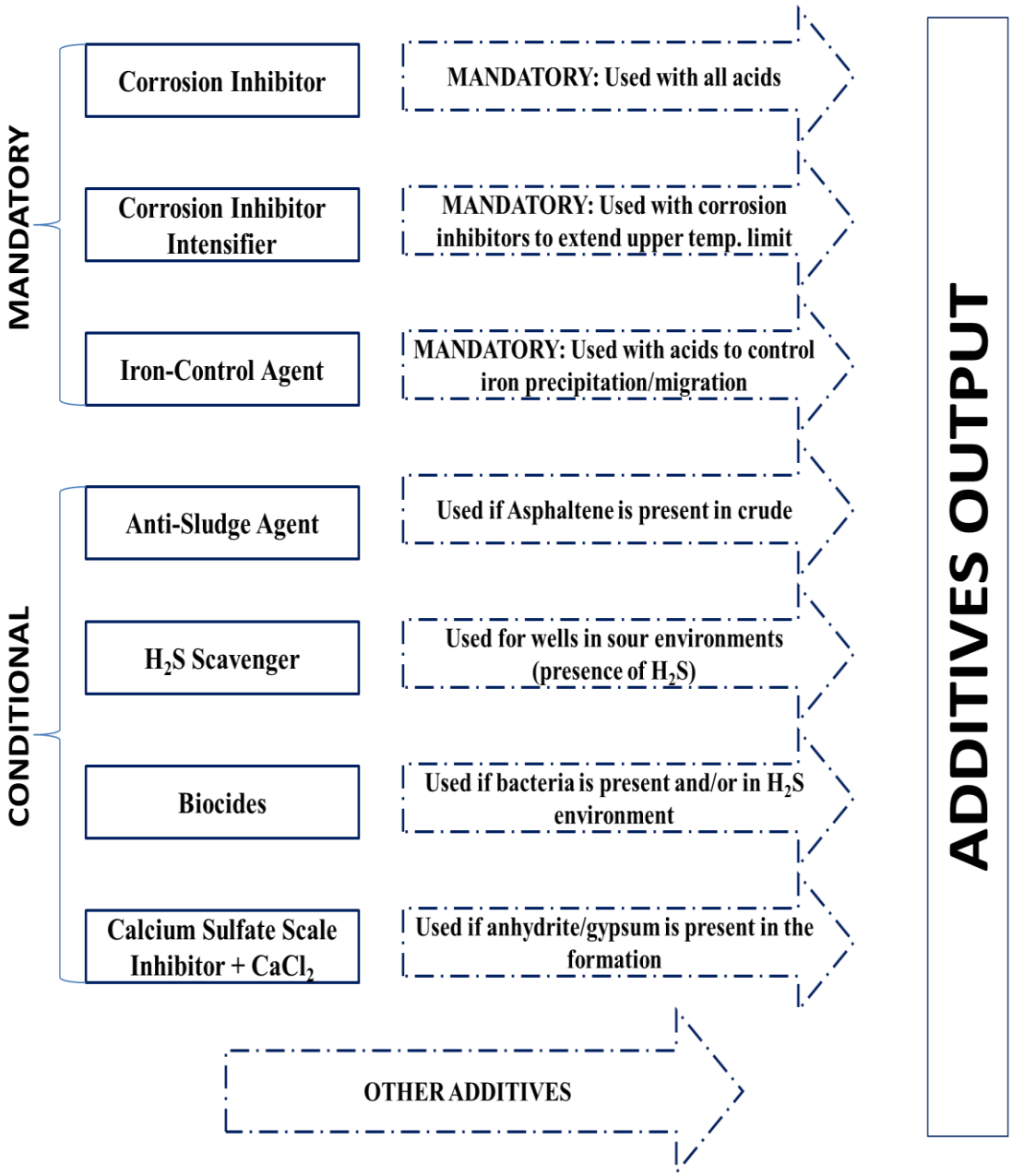

Fig. 6.2–Additives selection chart showing mandatory and conditional additives used during acid stimulation

7 CONCLUSIONS AND RECOMMENDATIONS

7.1. Conclusions

This study has analyzed existing carbonate acidizing models in the literature based on the approach to solution, and a modified two-scale model approach was used to study wormhole propagation during carbonate matrix acidizing. The two-scale model was then extended and applied to alternative acidizing fluids This work also considered the field scale application of existing models to predict the optimum injection and wormhole propagation rates. Lastly, an acidizing fluid and additives selection procedure was developed to aid in the proper design of a carbonate matrix acid treatment for optimal results based on the well and reservoir properties. The main results from this study are summarized below:

1. The Navier-Stokes momentum formulation effectively describes fluid flow in the two-scale carbonate acidizing model, and the model developed in this work captures all the dissolution patterns that occur during carbonate matrix acidizing. Sensitivity tests conducted on the model for various factors that affect wormhole propagation during carbonate acidizing provided results consistent with experimental observations and previous two-scale models with fluid flow described by Darcy's law.
2. At dissolution regimes above the optimum injection rate, the computational time by this model, with Navier-Stokes formulation, is significantly lower than the reported computational time by the models based on Darcy's law.

3. The simulation results from this study show that the geometry of flow influences wormhole propagation in the rock as well as the initial average porosity, formation heterogeneity, and core dimensions from laboratory experiments. From the combination of the above, the experimental results in the laboratory do not translate directly for field conditions and these factors should all taken into consideration when designing field treatments based on laboratory results.
4. The model output confirmed that reaction rate kinetics influence the wormholing process. The optimum injection rate increases as the reactivity of the acid, represented by the reaction rate constant, increases and the amount of acid required to achieve breakthrough is reduced. The significance of the effect of the order of reaction value on the PV_{BT} values was also demonstrated to highlight the importance of selecting the right parameters for the reaction kinetics of the carbonate acidizing model.
5. The modified two-scale model, which takes the dissociation equilibrium of weak acid into consideration in the reaction kinetics, provided simulated results for the acidizing of limestone with acetic acid that are consistent with reported experimental work.
6. The simulation results from application of the simplified first-order kinetics for chelating agents does not match reported experimental results due to the complex reaction involved in the dissolution of carbonates by chelates.

7.2. Limitations and Recommendations

The limitations of carbonates acidizing models are highlighted below with recommendations on the improvement of the two-scale model :

1. Most of the available carbonate matrix-acidizing models give good predictions of the dissolution structure, optimum injection, and/or wormhole propagation rates for coreflood tests in the laboratory, but the results do not translate directly for field applications.
2. For a field carbonate matrix acidizing treatment, it is recommended to inject the acidizing fluid at maximum allowable injection rates. The modified semi-empirical wormhole propagation model can be used for the calculation of wormhole growth rate to monitor skin evolution during treatment. The effect of additives on the dissolution rate of the acidizing fluid should be accounted for in translating the semi-empirical model.
3. To increase the accuracy of the two-scale model for chelating agents, a more detailed reaction kinetics to describe the multi-step chemistry at the solid-fluid interface is required.
4. The reduction in the computational power required for field scale application of the model can be investigated for a more representative description of wormhole propagation.

REFERENCES

Akanni, O.O. and Nasr-El-Din, H.A. 2015. The Accuracy of Carbonate Matrix-Acidizing Models in Predicting Optimum Injection and Wormhole Propagation Rates. Presented at the SPE Middle East Oil and Gas Show and Conference. Manama, Bahrain, 8–11 March. SPE 172575-MS. http://dx.doi.org/10.2118/172575-MS.

Ali, S.A. and Hinkel, J.J. 2000. Additives in Acidizing Fluids. In *Reservoir Stimulation*, ed. Economides, M.J. and Nolte, K.G., Chichester, UK: John Wiley and Sons.

ANSYS FLUENT. 2013. Canonsburg: ANSYS, Inc.

Balakotaiah, V. and West, D.H. 2002. Shape Normalization and Analysis of Mass Transfer Controlled Regime in Catalytic Monoliths. *Chem. Eng. Sc.* **57** (8): 1269-1286. http://dx.doi.org/10.1016/S0009-2509(02)00059-3.

Bazin, B. 2001. From Matrix Acidizing to Acid Fracturing: A Laboratory Evaluation of Acid/Rock Interactions. *SPE Prod & Fac* **16** (01): 22-29. SPE-66566-PA. http://dx.doi.org/10.2118/66566-PA.

Boles, J.L., Ke, M., and Parker, C. 2009. Corrosion Inhibition of New 15 Chromium Tubulars in Acid Stimulation Fluids at High Temperatures. Presented at the SPE Annual Technical Conference and Exhibition, New Orleans, Louisiana, 4–7 October. SPE-124887-MS. http://dx.doi.org/10.2118/124887-MS.

Brezinski, M.M. 1999. New Environmental Options for Corrosion Inhibitor Intensifiers. Presented at the SPE/EPA Exploration and Production Environmental Conference, Austin, Texas. 1–3 March. SPE 52707-MS. http://dx.doi.org/10.2118/52707-MS.

Bryant, S.L., Mellor, D.W., and Cade, C.A. 1993. Physically Representative Network Models of Transport in Porous Media. *AIChE J.* **39** (3): 387-396. http://dx.doi.org/10.1002/aic.690390303.

Buijse, M.A. 2000. Understanding Wormholing Mechanisms Can Improve Acid Treatments in Carbonate Formations. *SPE Prod & Oper* **15** (3): 168-175. SPE-38166-MS. http://dx.doi.org/10.2118/38166-MS.

Buijse, M.A. and Glasbergen, G. 2005. A Semiempirical Model to Calculate Wormhole Growth in Carbonate Acidizing. Presented at the Annual Technical Conference and Exhibition, Dallas, Texas, 9–10 October. SPE 96892-MS. http://dx.doi.org/10.2118/96892-MS.

Cassidy, J. 2006. Design and Investigation of a North Sea Acid Corrosion Inhibition System. NACE International NACE-06482.

Chang, C.L. and Fogler, H.S. 1994. Stabilization of Asphaltenes in Aliphatic Solvents Using Alkylbenzene-Derived Amphiphiles. 1. Effect of the Chemical Structure of Amphiphiles on Asphaltene Stabilization. *Langmuir* **10** (6): 1749-1757. http://dx.doi.org/10.1021/la00018a022.

Clapp, L.B. 1943. Sulfamic Acid and Its Uses. *J. Chem. Educ.* **20** (4): 189. http://dx.doi.org/10.1021/ed020p189.

Cohen, C.E., Ding, D., Quintard, M. et al. 2008. From Pore Scale to Wellbore Scale: Impact of Geometry on Wormhole Growth in Carbonate Acidization. *Chem Eng Sc* **63** (12) 3088. http://dx.doi.org/10.1016/j.ces.2008.03.021.

Daccord, G., Touboul, E., and Lenormand, R. 1989. Carbonate Acidizing: Toward a Quantitative Model of the Wormholing Phenomenon. *SPE Prod Eng* **4**(1): 63-68. SPE-16887-PA. http://dx.doi.org/10.2118/16887-PA.

Delorey, J.R., Allen, S., and McMaster, L. 1996. Precipitation of Calcium Sulfate During Carbonate Acidizing: Minimizing the Risk. Presented at the Petroleum Society of Canada Annual Technical Meeting, Calgary, Alberta, 10–12 June. PETSOC-96-84. http://dx.doi.org/10.2118/96-84.

De Oliveira, T.J.L., De Melo, A.R., Oliveira, J.A. et al. 2012. Numerical Simulation of the Acidizing Process and PVBT Extraction Methodology Including Porosity/Permeability and Mineralogy Heterogeneity. Presented at the International Symposium and Exhibition on Formation Damage Control. Lafayette, Louisiana. 15–17 January. SPE 151823-MS. http://dx.doi.org/10.2118/151823-MS.

Economides, M., Deimbachor, F.X., Brand, C.W. et al. 1991. Comprehensive Simulation of Horizontal-Well Performance. *SPE Form Eval* **6** (4): 418-426. http://dx.doi.org/10.2118/20717-PA.

Economides, M.J., Hill, A.D., Ehlig-Economides, C. et al. 1994. *Petroleum Production Systems*, first edition. Upper Saddle River, New Jersey: Prentice Hall PTR.

Fatt, I. 1956. The Network Model of Porous Media. I, II, III. *Pet. Trans. AIME* **207**: 144.

Fredd, C.N. and Fogler, H.S. 1999. Optimum Conditions for Wormhole Formation in Carbonate Porous Media: Influence of Transport and Reaction. *SPE J.* **4** (3): 196–205. SPE-56995-PA. http://dx.doi.org/10.2118/56995-PA.

Fredd, C.N. and Fogler, H.S. 1998. Influence of Transport and Reaction on Wormhole Formation in Porous Media. *AIChE J.* **44** (9): 1933. http://dx.doi.org/10.1002/aic.690440902.

Fredd, C.N. and Miller, M.J. 2000. Validation of Carbonate Matrix Stimulation Models. Presented at the International Symposium on Formation Damage Control, Lafayette, Louisiana, 23–24 February. SPE 58713-MS. http://dx.doi.org/10.2118/58713-MS.

Frenier, W.W. 1989. Acidizing Fluids Used to Stimulate High Temperature Wells Can Be Inhibited Using Organic Chemicals. Presented at the SPE International Symposium on Oilfield Chemistry, Houston, Texas, 8–10 February. SPE-18468-MS. http://dx.doi.org/10.2118/18468-MS.

Frenier, W.W., Fredd, C.N., and Chang, F. 2001b. Hydroxyaminocarboxylic Acids Produce Superior Formulations for Matrix Stimulation of Carbonates at High Temperatures. Presented at the SPE Annual Technical Conference and Exhibition, New Orleans, Louisiana, 30 September–3 October. SPE-71696-MS. http://dx.doi.org/10.2118/71696-MS.

Frenier, W.W. and Hill, D.G. 2002. Effect of Acidizing Additives on Formation Permeability During Matrix Treatments. Presented at the International Symposium and Exhibition on Formation Damage Control, Lafayette, Louisiana, 20–21 February. SPE-73705-MS. http://dx.doi.org/10.2118/73705-MS.

Frick, T.P., Kurmayr, M., and Economides, M.J. 1994. Modeling of Fractal Patterns in Matrix Acidizing and Their Impact on Well Performance. *SPE Prod & Oper* **9** (1): 61-68. SPE-23789-PA. http://dx.doi.org/10.2118/23789-PA.

Furui, K., Burton, R., Burkhead, D. et al. 2012. A Comprehensive Model of High-Rate Matrix-Acid Stimulation for Long Horizontal Wells in Carbonate Reservoirs: Part I--Scaling Up Core-Level Acid Wormholing to Field Treatments. *SPE J.* **17**(1), 271-279. http://dx.doi.org/10.2118/134265-PA.

Gdanski, R. 1999. A Fundamentally New Model of Acid Wormholing in Carbonates. Presented at the SPE European Formation Damage Conference, The Hague, Netherlands, 31 May–1 June. SPE 54719-MS. http://dx.doi.org/10.2118/54719-MS.

Glasbergen, G., Kalia, N., and Talbot, M.S. 2009. The Optimum Injection Rate for Wormhole Propagation: Myth or Reality? Presented at the 8th European Formation Damage Conference, Scheveningen, 27–29 May. SPE 121464-MS. http://dx.doi.org/10.2118/121464-MS.

Golfier, F., Zarcone, C., Bazin, B. et al. 2002. On The Ability of a Darcy-Scale Method Model to Capture Wormhole Formation During the Dissolution of a Porous Medium. *J. Fluid Mech* **457**: 213-254. http://dx.doi.org/10.1017/S0022112002007735.

Gong, M, and El-Rabba, A.M. 1999. Quantitative model of wormholing process in carbonate acidizing. Presented at the Mid-Continent Operations Symposium, Oklahoma City, Oklahoma, 18–21 February. SPE 52165-MS. http://dx.doi.org/10.2118/52165-MS.

Gupta, N. and Balakotaiah, V. 2001. Heat and Mass Transfer Coefficients in Catalytic Monoliths. *Chem. Eng. Sc.* **56** (16): 4771-4786. http://dx.doi.org/10.1016/S0009-2509(01)00134-8.

Hashmi, S.M. and Firoozabadi, A. 2011. Tuning Size and Electrostatics in Non-Polar Colloidal Asphaltene Suspensions by Polymeric Adsorption. *Soft Matter* **7** (18): 8384–8391. http://dx.doi.org/10.1039/c1sm05384a.

Hinshaw, E., Gambale, D., and Chambers, B. 2011. Evaluation of Corrosion Resistant Alloys for Deep Well Acidizing Environments. Corrosions Solutions Conference, Lake Louise, Alberta, Canada, 25–30 September.

Hoefner, M.L. and Fogler, H.S. 1988. Pore Evolution and Channel Formation during Flow and Reaction in Porous Media. *AIChE J.* **34** (1): 45-54. http://dx.doi.org/10.1002/aic.690340107.

Houchin, L.R., Dunlap, D.D., Arnold, B.D. et al. 1990. The Occurrence and Control of Acid-Induced Asphaltene Sludge. Presented at the SPE Formation Damage Control Symposium, Lafayette, Louisiana, 22–23 February. SPE-19410-MS. http://dx.doi.org/10.2118/19410-MS.

Huang, T., Hill, A.D., and Schechter, R.S. 1997. Reaction Rate and Fluid Loss: The Keys to Wormhole Initiation and Propagation in Carbonate Acidizing. Presented at the International Symposium on Oilfield Chemistry, Houston, Texas, 18–21 February. SPE 37312-MS. http://dx.doi.org/10.1016/10.2118/37312-MS.

Huang, T., Zhu, D., and Hill, A.D. 1999. Prediction of Wormhole Population Density in Carbonate Matrix Acidizing. Presented at the SPE European Formation Damage Conference, The Hague, Netherlands, 31 May–1 June. SPE 54723-MS. http://dx.doi.org/10.2118/54723-MS.

Hung, K.M., Hill, A.D., and Sepehrnoori, K. 1989. A Mechanistic Model of Wormhole Growth in Carbonate Matrix Acidizing and Acid Fracturing. *J Pet Technol* **41** (1): 59-66. SPE-16886-PA. http://dx.doi.org/2118/16886-PA.

Izgec, O., Zhu, D., & Hill, A. D. 2010. Numerical and Experimental Investigation of Acid Wormholing during Acidization of Vuggy Carbonate Rocks. *J. Pet. Sci. Eng.* **74** (1): 51-66. http://dx.doi.org/10.1016/j.petrol.2010.08.006

Kalia, N. and Balakotaiah, V. 2007. Modeling and Analysis of Wormhole Formation in Reactive Dissolution of Carbonate Rocks. *Chem. Eng. Sc.* **62** (4): 919-928. http://dx.doi.org/10.1016/j.ces.2006.10.021.

Kalia, N. and Balakotaiah, V. 2009. Effect of Medium Heterogeneities on Reactive Dissolution of Carbonates. *Chem. Eng. Sc.* **64** (2): 376-390. http://dx.doi.org/10.1016/j.ces.2008.10.026.

Kalia, N. and Glasbergen, G. 2009. Wormhole Formation in Carbonates under Varying Temperature Conditions. Presented at the 8th European Formation Damage Conference. Scheveningen, The Netherlands, 27–29 May. SPE 121803-MS. http://dx.doi.org/10.2118/121803-MS.

Ke, M. and Boles, J. 2004. Corrosion Behavior of Various 13 Chromium Tubulars in Acid Stimulation Fluids. Presented at the SPE International Symposium on Oilfield Corrosion, Aberdeen, United Kingdom, 28 May. SPE-87561-MS. http://dx.doi.org/10.2118/87561-MS.

Kuchuk, F.J., Goode, P.A., Brice, B.W. et al. 1990. Pressure-Transient Analysis for Horizontal Wells. *J Pet Technol* **42** (8): 974-979, 1028-1031. http://dx.doi.org/10.2118/18300-PA.

Lalchan, C., O'Neil, B., and Maley, D. 2013. Prevention of Acid Induced Asphaltene Precipitation: A Comparison of Anionic Vs. Cationic Surfactants. Presented at the 2013 SPE International Symposium on Oilfield Chemistry, The Woodlands, TX, USA, 8–10 April. SPE-164087-MS. http://dx.doi.org/10.2118/164087-MS.

Li, L., Nasr-El-Din, H., Chang, F., and Lindvig, T. 2008. Reaction of Simple Organic Acids and Chelating Agents with Calcite. Presented at the International Petroleum Technology Conference. Kuala Lumpur, Malaysia. 2–5 December. IPTC-12886-MS. http://dx.doi.org/10.2523/12886-MS.

Liu, M., Zhang, S., and Mou, J. 2012. Effect of Normally Distributed Porosities on Dissolution Pattern in Carbonate Acidizing. *J. Pet. Sci. Eng.* **94–95** (0): 28-39. http://dx.doi.org/10.1016/j.petrol.2012.06.021.

Liu, X., Ormond, A., Bartko, K. et al. 1997. A Geochemical Reaction-Transport Simulator for Matrix Acidizing Analysis and Design. *J. Pet. Sci. Eng.* **17** (1–2): 181-196. http://dx.doi.org/10.1016/S0920-4105(96)00064-2.

Lund, K., Fogler, H.S., and McCune, C.C. 1973. Acidization—I. The Dissolution of Dolomite in Hydrochloric Acid. *Chem. Eng. Sc.* **28** (3): 691-IN691. http://dx.doi.org/10.1016/0009-2509(77)80003-1.

Maheshwari, P. and Balakotaiah, V. 2013. Comparison of Carbonate HCl Acidizing Experiments with 3D Simulations. *SPE Prod & Oper* **28** (04): 402-413. SPE-164517-PA http://dx.doi.org/10.2118/164517-PA.

Maheshwari, P., Maxey, J., and Balakotaiah, V. 2014. Simulation and Analysis of Carbonate Acidization with Gelled and Emulsified Acids. Presented at the Abu Dhabi International Petroleum Exhibition and Conference. Abu Dhabi, UAE, 10–13 November. SPE 171731-MS. http://dx.doi.org/10.2118/171731-MS.

Maheshwari, P., Ratnakar, R.R., Kalia, N. et al. 2012. 3-D Simulation and Analysis of Reactive Dissolution and Wormhole Formation in Carbonate Rocks. *Chem. Eng. Sc.* **90** (0): 258–274. http://dx.doi.org/10.1016/j.ces.2012.12.032.

Mahmoud, M.A. and Nasr-El-Din, H.A. 2012. Modeling of the Flow of Chelating Agents in Porous Media in Carbonate Reservoirs Stimulation. Presented at the North Africa Technical Conference and Exhibition, Cairo, Egypt, 20–22 February. SPE-150065-MS. http://dx.doi.org/10.2118/150065-MS.

Metcalf, A.S. 1998. Environment and Coiled Tubing: Both Can Be Protected. Presented at the SPE Eastern Regional Meeting, Pittsburgh, Pennsylvania, 9–11 November. SPE-51095-MS. http://dx.doi.org/10.2118/51095-MS.

Panga, M.K.R., Ziauddin, M., and Balakotaiah, V. 2005. Two-Scale Continuum Model for Simulation of Wormholes in Carbonate Acidization. *AIChE J.* **51** (12): 3231–3248. http://dx.doi.org/10.1002/aic.10574.

Panga, M., Ziauddin, M., Gandikota, R., and Balakotaiah, V. 2004. A New model for Predicting Wormhole Structure and Formation in Acid Stimulation of Carbonates. Presented at the SPE International Symposium and Exhibition on Formation Damage Control. Lafayette, Louisiana, 18–20 February. SPE 86517-MS. http://dx.doi.org/10.2118/86517-MS

Panga, M.K.R., Balakotaiah, V., and Ziauddin, M. 2002. Modeling, Simulation and Comparison of Models for Wormhole Formation during Matrix Stimulation of Carbonates. Presented at the SPE Annual Technical Conference and Exhibition. San Antonio, Texas. 29 September–2 October. SPE 77369-MS http://dx.doi.org/10.2118/77369-MS.

Ratnakar, R.R., Kalia, N., and Balakotaiah, V. 2012. Carbonate Matrix Acidizing with Gelled Acids: An Experiment-Based Modeling Study. Presented at the SPE International Production and Operations Conference and Exhibition. Doha, Qatar, 14–16 February. SPE 154936-MS. http://dx.doi.org/10.2118/154936-MS.

Rose, W. 1957. Studies of Waterflood Performance: Use of Network Models, III. *St Geolog Surv Circ* **237** (1).

Rowan, G. 1959. Theory of acid treatment of limestone formations. *J. Inst. Petrol.* **45** (431).

Sahimi, M., Gavalas, G.R., and Tsotsis, T.T. 1990. Statistical and Continuum Models of Fluid-Solid Reactions in Porous Media. *Chem. Eng. Sc.* **45** (6): 1443-1502. http://dx.doi.org/10.1016/0009-2509(90)80001-u.

Schechter, R.S. 1992. *Oil Well Stimulation*, original edition. Englewood Cliffs, New Jersey: Prentice Hall.

Schechter, R.S. and Gidley, J.L. 1969. The Change in Pore Size Distribution from Surface Reactions in Porous Media. *AIChE J.* **15** (3): 339-350. http://dx.doi.org/10.1002/aic.690150309.

Sengul, M. and Remisio, L.H.A. 2002. Applied Carbonate Stimulation - an Engineering Approach. Presented at the Abu Dhabi International Petroleum Exhibition and Conference, Abu Dhabi, United Arab Emirates, 13–16 October. SPE-78560-MS. http://dx.doi.org/10.2118/78560-MS.

Seth, K., Evans, B.A., and Gabrysch, A.D. 2011. Development and Testing of a Novel Corrosion Inhibitor Technology for Acid Corrosion. Presented at the SPE Middle East Oil and Gas Show and Conference, Manama, Bahrain, 25–28 September. SPE-142675-MS. http://dx.doi.org/10.2118/142675-MS.

Simon, R. and Kelsey, F.J. 1972. The Use of Capillary Tube Networks in Reservoir Performance Studies: II. Effect of heterogeneity and mobility on miscible displacement efficiency. *SPE J.* **12** (04): 345-351. SPE-3482-PA. http://dx.doi.org/10.2118/3482-PA.

Smith, C.F., Dollarhide, F.E., and Byth, N.J. 1978. Acid Corrosion Inhibitors - Are We Getting What We Need? *J Pet Technol* **30** (5): 737-746. http://dx.doi.org/10.2118/5644-PA.

Strassner, J.E. 1968. Effect of pH on Interfacial Films and Stability of Crude Oil-Water Emulsions. *J Pet Technol* **20** (3): 303-312. http://dx.doi.org/10.2118/1939-PA.

Taylor, K.C., Al-Ghamdi, A.H., and Nasr-El-Din, H.A. 2004. Effect of Additives on the Acid Dissolution Rates of Calcium and Magnesium Carbonates. *SPE Prod & Oper* **19** (3): 122-127. http://dx.doi.org/10.2118/80256-PA.

Thomas, R.L. and Morgenthaler, L.N. 2000. Introduction to Matrix Treatments. In *Reservoir Stimulation*, ed. Economides, M.J. and Nolte, K.G. Chichester, England: Wiley.

Thompson, K.E. and Fogler, H.S. 1997. Modeling Flow in Disordered Packed Beds from Pore-Scale Fluid Mechanics. *AIChE J.* **43** (6): 1377–1389. http://dx.doi.org/10.1002/aic.690430602.

Van Domelen, M.S. and Jennings, A.R. 1995. Alternate Blends for HPHT Applications. Presented at the Offshore Europe Conference held in Aberdeen, Scotland. September 5–8. SPE-30419-MS. http://dx.doi.org/10.2118/30419-MS.

Vik, B., Djurhuus, K., Spildo, K., and Skauge, A. 2007. Characterisation of Vuggy Carbonates. Presented at the SPE/EAGE Reservoir Characterization and Simulation Conference, Abu Dhabi, UAE, 28–31 October. SPE-111434-MS. http://dx.doi.org/10.2118/111434-MS.

Wang, Y., Hill, A.D., and Schechter, R.S. 1993. The Optimum Injection Rate for Matrix Acidizing of Carbonate Formations. Presented at the SPE Annual Technical Conference and Exhibition, Houston, Texas, 3–6 October. SPE 26578-MS. http://dx.doi.org/10.2118/26578-MS.

Welton, T., and Van Domelen, M. 2008. High-Viscosity-Yield Acid Systems for High-Temperature Stimulation. *SPE Prod & Oper* **23** (2), 177-183. http://dx.doi.org/10.2118/98237-PA.

Wu, Y.T. and Grant, C. 2002. Effect of Chelation Chemistry of Sodium Polyaspartate on the Dissolution of Calcite. *Langmuir* **18** (18): 6813-6820. http://dx.doi.org/10.1021/la011839a.

Zhang, Y., Yang, S., Zhang, S. et al. 2014. Wormhole Propagation Behavior and Its Effect on Acid Leakoff under In Situ Conditions in Acid Fracturing. *Transport Porous Med* **101** (1): 99-114. http://dx.doi.org/10.1007/s11242-013-0233-z.

APPENDIX

SUMMARIZED CORROSION RATES

		N80		13Cr		22Cr	
	Author	**Temp (°F)**	**Rate (lb/ft^2/test period)**	**Temp (°F)**	**Rate (lb/ft^2/test period)**	**Temp (°F)**	**Rate (lb/ft^2/test period)**
15 wt% HCl	(Cassidy 2006)	338	0.006 (8 hrs)	300	0.007 (8 hrs)		
		400	0.005 (3 hrs)				
	(Metcalf 1998)	290	0.029 (6 hrs)	270	0.052 (6 hrs)		
		310	0.044 (6 hrs)	310	0.050 (6 hrs)		
	(Smith et al. 1978) *	250	0.035 (6 hrs)				
		350	0.035 (1 hr)				
	(Ke and Boles 2004)			260	0.013 (6hrs)		
	(Frenier 1989)	375	0.046 (4 hrs)	375	0.066 (4 hrs)		
		400	0.055 (4 hrs)	400	0.07 (4 hrs)		
	(Seth et al. 2011)			220	0.0162 (24 hrs)	220	0.0225 (24 hrs)
	(Boles et al. 2009)			260	0.013 (6 hrs)		
				350	0.039 (6 hrs)		
28 wt% HCl	(Welton and Domelen 2008)	290	0.028				
	(Smith et al. 1978) *	250	0.067 (3 hrs)				
		350	0.102 (1 hr)				
	(Frenier 1989)	300	0.025 (8 hrs)				
		320	0.05 (8 hrs)				
		340	0.125 (8 hrs)				
10 wt% HCl	(Ke and Boles 2004)			260	0.006 (6 hrs)		
	(Boles et al. 2009)			260	0.011 (6 hrs)		